Assessing the accuracy of 1-D analytical heat tracing for estimating near-surface sediment thermal diffusivity and water flux under transient conditions

Rau, Gabriel C.; Cuthbert, Mark O.; McCallum, Andrew M.; Halloran, Landon J S; Andersen, Martin S.

DOI:
10.1002/2015JF003466

Document Version
Peer reviewed version

Citation for published version (Harvard):
Rau, GC, Cuthbert, MO, McCallum, AM, Halloran, LJS & Andersen, MS 2015, 'Assessing the accuracy of 1-D analytical heat tracing for estimating near-surface sediment thermal diffusivity and water flux under transient conditions', *Journal of Geophysical Research: Earth Surface*, vol. 120, no. 8, pp. 1551-1573. https://doi.org/10.1002/2015JF003466

Assessing the accuracy of 1-D analytical heat tracing for estimating near-surface sediment thermal diffusivity and water flux under transient conditions

Revised manuscript for resubmission to the *Journal of Geophysical Research (Earth Surface)*

Gabriel C. Rau[*,1], Mark O. Cuthbert[1, 2], Andrew M. McCallum[3], Landon J.S. Halloran[1], Martin S. Andersen[1]

1. Connected Waters Initiative Research Centre, School of Civil and Environmental Engineering, Water Research Laboratory, UNSW Australia, Manly Vale 2093 NSW, Sydney, Australia
2. School of Geography, Earth and Environmental Sciences, University of Birmingham, Edgbaston, Birmingham, B15 2TT, UK
3. Affiliated with the Connected Waters Initiative Research Centre, UNSW Australia, Manly Vale, Australia

* Corresponding Author:

Gabriel C. Rau (gabriel.rau@unsw.edu.au)

UNSW Australia, Water Research Laboratory, 110 King Street, Manly Vale 2093, Australia

Phone: +61 2 8071 9850, Fax: +61 2 9949 4188

Keywords: Heat as a tracer, scour/depositional processes, transient water flux, temperature records, harmonic signal extraction.

Abstract

Amplitude decay and phase delay of oscillating temperature records measured at two vertical locations in near-surface sediments can be used to infer transient water fluxes, thermal diffusivity and sediment scour/deposition. While methods that rely on the harmonics-based analytical heat transport solution assume a steady-state water flux, many applications have reported transient fluxes, but ignored the possible violation of this assumption in the method. Here, we use natural heat tracing as an example to investigate the extent to which changes in the water flux, and associated temperature signal non-stationarity, can be separated from other influences. We systematically scrutinize the assumption of steady-state flow in analytical heat tracing and test the capabilities of the method to detect the timing and magnitude of flux transients. A numerical model was used to synthesize the temperature response to different step and ramp changes in advective thermal velocity magnitude and direction for both a single-frequency and multi-frequency temperature boundary. Time-variable temperature amplitude and phase information were extracted from the model output with different signal processing methods. We show that a worst-case transient flux induces a temperature non-stationarity, the duration of which is less than 1 cycle for realistic sediment thermal diffusivities between 0.02-0.13 m^2/d. However, common signal processing methods introduce erroneous temporal spreading of advective thermal velocities and significant anomalies in thermal diffusivities or sensor spacing, which is used as an analogue for streambed scour/deposition. The most time-variant spectral filter can introduce errors of up to 57 % in velocity and 33 % in thermal diffusivity values with artifacts spanning ±2 days around the occurrence of rapid changes in flux. Further, our results show that analytical heat tracing is unable to accurately resolve highly time-variant fluxes and thermal diffusivities and does not allow for the inference of scour/depositional processes due to the limitations of signal processing in disentangling flux-related signal non-stationarities from those stemming from other sources. To prevent erroneous interpretations, hydrometric data should always be acquired in combination with temperature records.

1. Introduction

Many measured signals that fluctuate over time exhibit amplitude decay and phase shifting over space caused by time-varying natural processes, for example: seismic wave propagation [Best et al., 1994], depth profiles of soil moisture [Wu et al., 2002], groundwater levels [Cuthbert, 2010] and seafloor temperature depth profiles [Goto et al., 2005]. In water-saturated near-surface aquatic systems natural heat has become a popular tracer to quantify vertical water fluxes [Anderson, 2005; Rau et al., 2014]. This is due to the presence of daily temperature fluctuations on the earth's surface [Stallman, 1965], increasing interest in surface-groundwater exchange fluxes, and developments in measurement technology to miniaturize and automate sensors [Constantz, 2008]. In particular, analytical approaches to invert water fluxes from multi-level temperature records have received much attention and are now common practice. Constantz [2008] correctly predicted that heat tracing will elevate the significance of streambed research to a field of "streambed science".

Few publications in this field of research have sparked as much follow-on research as Suzuki's [1960] and Stallman's [1965] original presentation of the analytical solution to the 1D convective-conductive heat transport equation with a sinusoidal temperature boundary at the top and a constant temperature boundary at infinite depth. Stallman's [1965] model is an extension to the harmonically-forced solution developed by Carslaw and Jaeger [1959], allowing for movement of water by including the first order spatial derivative of temperature. As such, it could be a mathematical description for many physical processes that are gradient driven and adhere to a simplified homogeneous linear second order differential equation.

Stallman's [1965] analytical solution has inspired various method developments and applications. Goto et al. [2005] successfully estimated sediment thermal regimes and the steady-state vertical water flux near a hydrothermal mound at the ocean floor. Hatch et al. [2006] dissected the original analytical solution to estimate time variable fluxes from the amplitude damping and the phase shifting, both contained in the temperature signal over depth. Keery et al. [2007] calculated streambed vertical fluxes using the amplitude damping feature of the temperature-depth record. They extracted the daily sinusoidal component from noisy field records using Dynamic Harmonic Regression (DHR) [Young et al., 1999; Taylor et al., 2007]. McCallum et al. [2012] recombined the two sinusoid features, amplitude and phase, to arrive at two unknowns, streambed thermal diffusivity and advective thermal velocity. Luce et al. [2013] revisited the original differential equation and combined the information contained in amplitude and phase to derive explicit analytical solutions for sensor spacing or streambed thermal

diffusivity as well as advective thermal velocity. These papers contain a wealth of methods that can be readily applied to estimate streambed thermal regimes and vertical water fluxes.

Further investigated were the impact of parameter uncertainty and non-ideal conditions (such as sediment heterogeneity and a 2D flow field) on the flux results [Lautz, 2010; Shanafield et al., 2011; Roshan et al., 2012; Cuthbert and Mackay, 2013; Irvine et al., 2015]. The increasing popularity of analytical heat tracing methods has led to the development of algorithms that automate the flux quantification from temperature records, namely *Ex-Stream* [Swanson and Cardenas, 2011] and *VFLUX* [Gordon et al., 2012]. These methods are implicitly geared towards quantifying flux time series.

What is often overlooked or implicitly assumed in papers that apply methods to quantify fluxes and thermal diffusivities from field temperature records is the fact that the original analytical solution is based on the assumption of steady-state flow. This assumption is in contrast to the aim of understanding natural processes that are commonly transient in nature. While Lautz [2012] experimented in the laboratory with transient fluxes and found that diurnally forced analytical solutions are able to offer sub-daily fluxes in reasonable agreement with the known fluxes of the experiments, McCallum et al. [2012] concluded from field studies that rapid changes in hydraulic forcing (i.e. floods) lead to erroneous fluxes due to violation of the method assumptions. Furthermore, a reversal in the flux direction, as expected during flood events (e.g. the nature of the flood hydrograph as well as return flow of bank storage), complicates the system's thermal response (i.e. memory effect). We suggest that this will lead to potentially flawed flux estimates when quantified using heat tracing methods based on the assumption of harmonic temperature data. This scenario and its implications on heat tracing have not been comprehensively investigated. However, testing the reliability of heat tracing under highly transient flux scenarios is a crucial prerequisite for its further application in advancing process understanding.

The aim of this paper is to explore how accurately flux transients can be determined with methods based on harmonic features that are embedded in temperature records (analytical heat tracing). We systematically test a) the streambed thermal response time to flux transients, and b) the accuracy of the water flux, thermal diffusivity and sediment scour/deposition time series inverted with analytical heat tracing. We demonstrate that near-surface sediment has a particular thermal response time to sudden flux transients, i.e. quantifiable time between flux-related thermal disturbance and return to stationarity. Further, we distinguish between the basic thermal response to a harmonic driver and impacts caused by extraction of fixed-frequency harmonic

components that stem from general non-stationarity and transients in vertical fluxes, including reversals. Finally, we provide guidance under which conditions the quantification of time-variable water flux, thermal diffusivity or sediment scour/deposition from temperature records in combination with diurnally forced analytical solutions are reliable. Our results are generic and could be useful to other areas of geophysics that utilize time-frequency transformation or amplitude and phase extraction of periodically fluctuating signals to quantify natural processes or properties.

2. Methodology

2.1. Harmonically forced analytical solutions

This investigation is based on the 1D conductive-convective heat transport equation which is discussed in detail in a number of papers [e.g., Suzuki, 1960; Stallman, 1965; Anderson, 2005; Constantz, 2008; Rau et al., 2014] and it will therefore not be stated here again. Rather, we focus on the analytical methods derived from the original solution by Suzuki [1960] and Stallman [1965]. An analytical solution for the propagation of a harmonic temperature signal with depth is given as [Goto et al., 2005]

$$T(z,t)=\sum_{i=1}^{n} A_i \cdot \exp\left(\frac{v_t z}{2D}-\frac{z}{2D}\sqrt{\frac{\alpha_i+v_t^2}{2}}\right)\cdot\cos\left(\frac{2\pi}{P_i}t-\frac{z}{2D}\sqrt{\frac{\alpha_i-v_t^2}{2}}\right) \quad (1)$$

where

$$\alpha_i=\sqrt{v_t^4\left(1+\left(\frac{8\pi D}{P_i v_t^2}\right)^2\right)}. \quad (2)$$

Here, T is the temperature in the sediment at depth z [L] below the surface, and t [T] is the time. The subscript i represents individual harmonic frequency components with a total of n components. A_i is the temperature amplitude [K], and P_i is the period [T] of the harmonic component i (frequency $f=1/P$ or angular frequency $\omega=2\pi/P$). The parameter of interest is the 'advective thermal velocity' v_t [L/T], as it is proportional to the vertical flux (see further below). D [L^2/T] is the effective thermal diffusivity but without the influence of thermal dispersivity as this has been found insignificant for fluxes smaller than ~10 m/d [Rau et al., 2012a]. However, Rau et al. [2012b] reported that D can be underestimated due to additional thermal spread originating from transverse temperature gradients when the solution requires the dimensionality to be reduced to 1-D, even in materials that are considered homogeneous.

142 Equation 1 follows the principle of superposition (Fourier's theorem), which is inherent to the
143 linear heat transport differential equation, and allows isolation of the signal's different sinusoidal
144 components [Goto et al., 2005].

145 The following reviews and summarizes the general approach that is used to quantify vertical
146 fluxes using Equation 1. Options for extracting amplitude and phase of the diel temperature
147 harmonic from noisy temperature time series with different signal processing methods will be
148 discussed later. The advantage of a harmonic signal is that it has two distinct features, amplitude
149 and phase, which allows solving for two unknowns. For a pair of temperature sensors located at
150 different depths (z positive upwards, negative downwards, $z_2 < z_1$) the temperature amplitude
151 ratio A_r and phase shift $\Delta\phi$ (in radians or days) are defined as [Stallman, 1965; Hatch et al.,
152 2006]

153 (3) $$A_r = \frac{A_2}{A_1}$$

154 (4) $$\Delta\phi = \phi_2 - \phi_1$$

155 Stallman [1965] reported that the sinusoidal temperature signal dampens and shifts phase over
156 depth (Figure 1).

157 Hatch et al. [2006] used both features, amplitude ratio and phase shift, separately to solve for the
158 vertical advective thermal velocity

159 (5) $$v_{t,Ar} = \frac{2D}{\Delta z}\ln\left(A_r\right) + \sqrt{\frac{\alpha + v_{t,Ar}^2}{2}}$$

160 (6) $$v_{t,\Delta\phi} = \sqrt{\alpha - 2\left(\frac{4\Delta\phi\pi D}{P\Delta z}\right)^2}$$

161 When using Equations 5-6 the disadvantage is that the thermal diffusivity must be known before
162 calculating velocities as it significantly influences the results [Hatch et al., 2010]. Equations 5-6
163 were field tested and results by the two equations were found to differ significantly from each
164 other despite relying on the same thermal parameters [Rau et al., 2010].

165 Luce et al. [2013] revisited Stallman's [1965] original solution and found that amplitude and
166 phase can be combined and expressed as dimensionless velocity as

167 (7) $$\eta = -\frac{ln\left(A_r\right)}{\Delta\phi}.$$

The combined information in Equation 7 is the ratio between the advective (v_t) and the diffusive (v_d) thermal velocity, as

$$v^* = \frac{v_t}{v_d} = \frac{1-\eta^2}{\sqrt{2\eta\left(1+\eta^2\right)}} = \frac{Pe}{2}. \quad (8)$$

Conveniently, Pe is the thermal Péclet number indicating dominance of diffusive ($Pe < 1$) or convective conditions ($Pe > 1$). Equation 7 is useful to determine the direction and change of water velocity simply from temperature amplitude and phase information without any further parameters, such as sensor spacing or thermal diffusivity [Luce et al., 2013].

The damping depth z_d of the sinusoid is determined as [Goto et al., 2005; Luce et al., 2013]

$$z_d = \sqrt{\frac{DP}{\pi}}. \quad (9)$$

This is the depth at which the temperature amplitude is damped to $1/e$ of its original value. Assuming a constant sensor spacing (Δz), the thermal diffusivity can be calculated using [Luce et al., 2013]

$$D = \frac{2\pi\eta\Delta z^2}{P\left(ln^2\left(A_r\right)+\Delta z^2\right)} \quad (10)$$

It is noteworthy that results from this equation are equivalent to that published by McCallum et al. [2012]. They reported that the thermal diffusivity calculated using field data can exceed physically possible values during periods when the stream stage rapidly changes (transient flux conditions). While they suggested that the method may break down during such conditions, they did not investigate its limitations in correctly resolving parameters over the duration of transient conditions.

Analogously, assuming a constant thermal diffusivity (D), the sensor spacing (Δz) is determined as [Luce et al., 2013; Tonina et al., 2014]

$$\Delta z = z_d\sqrt{\frac{ln^2\left(A_r\right)+\Delta\phi^2}{2\eta}} \quad (11)$$

Interestingly, Luce et al. [2013] and Tonina et al. [2014] have used this to quantify sediment scour/depositional processes, indicated by a time variable sensor spacing, based on field data obtained during a period of transient stream discharge. However, they did not consider the

possible limitations that transient fluxes can impose on methods based on the diurnal heat forcing. Here, it is important to note that equations 10 and 11 are exactly the same and can either quantify sediment thermal diffusivity (D) or scour/depositional processes inferred from sensor spacing (Δz).

Finally, the advective thermal velocity is determined using [Luce et al., 2013]

$$v_t = \frac{2\pi\Delta z\left(1-\eta^2\right)}{P\sqrt{\left(1+\eta^2\right)\left(ln^2\left(A_r\right)+\Delta z^2\right)}}. \quad (12)$$

Equation 13 is the final step to quantify the Darcy flux (q) from advective thermal velocity as

$$q = \left(\varepsilon + \left(1-\varepsilon\right)\frac{c_s^v}{c_w^v}\right)v_t \quad (13)$$

where additional sediment properties are required: ε is the porosity of the sediment, c_s^v and c_w^v are the volumetric heat capacities of the solids and water, respectively. Equation 13 is stated here for sake of completeness, but will not be used further to quantify the Darcy flux, since this is not the aim of the paper. Instead, we let the advective thermal velocity, v_t, represent the convective conditions (vertical flux magnitude and direction). In this paper we use Equations 3-12 to invert fluxes from temperature data that has been generated by a numerical model described in the next section.

2.2. Numerical modeling

In this paper a transient numerical model was used to generate the thermal response $T(z,t)$ to step and ramp changes in the water velocity (i.e. worst case transient scenario). The conceptual model is a diurnally forced water saturated near-surface system (i.e. like a streambed). The approach is an analogue to any real-world transient flux signal, as this can be thought of as multiple discrete-time steps with variable magnitudes and durations.

COMSOL Multiphysics V5 [COMSOL, 2014] was used as the numerical solver for the conductive-convective heat transport equation in a one-dimensional domain, resembling the vertical extent of a near-surface hydrologic system. For all simulations a sinusoidal temperature signal with period $P = 1$ day and amplitude of 3 °C at a mean of 20 °C was applied at the top of the domain. The bottom of the domain was held at a constant temperature of 20 °C at a large enough distance (30 m) to have no further effect on the simulated temperatures in the upper 1 m

used in the analysis. The initial condition was T = 20 ºC across the whole model domain. The mesh increased in size from 4 mm at the upper boundary to 1 cm at the base of the domain. The absolute solver tolerance was set to $1 \cdot 10^{-5}$ ºC with a relative tolerance of $1 \cdot 10^{-9}$, small enough to ensure that the model output was no longer sensitive to changes in these values. The numerical models were accurate to within ~0.0001 °C against the range of analytical models during steady velocity periods.

Each simulation was conducted for a total time of 30 days with a constant advective thermal velocity assigned to the first 10 days, followed by a step change in advective thermal velocity and another 20 days of simulation. Temperature records were generated at 96 time steps per day (15 min time step) at the top boundary and at the depths: 0.02 m, 0.05 m, 0.1 m, 0.2 m, 0.3 m, 0.5 m, 0.75 m and 1 m (see dashed horizontal lines in Figure 1). The large number of depths allowed investigation of both up- and downward flow by evaluating data from sensor locations at depths where the temperature signal was not damped beyond recognition (temperature variations well above the limits of typical field instrument resolution, typically 0.001-0.01 ºC).

The following transient advective thermal velocity scenarios were simulated in separate sub cases:

1. 0 m/d followed by a downward step change: -0.01, -0.1, -0.5, -1 and -5 m/d,
2. 0 m/d followed by an upward step change: 0.01, 0.1, 0.5, 1 and 2 m/d,
3. Reversal step change from -1 m/d downwards to 1 m/d upwards, and from 1 m/d upwards to -1 m/d downwards,
4. Linear increase from 0 to -1 m/d within a time of 0.5, 1, 2 and 4 days.

The velocity reversals are particularly interesting as the thermal signal is transported downwards and then upwards (or vice versa) by the water flux by convection while conducting simultaneously depending on the temperature-depth gradient. The linear streambed velocity increases represent the likely responses to different hydrograph characteristics, for example fast flux transient caused by flash flooding, or slow flux transients due to snow melt.

To illustrate the influence of the thermal diffusivity on the results, all cases were simulated for physically realistic minimum and a maximum thermal diffusivity as reported in the literature [i.e., Shanafield et al., 2011; McCallum et al, 2012]. The numerically simulated temperature time series were first processed using different signal extraction methods, and then Equations 3-12 were used to invert for time series of transient velocities and thermal diffusivities. To provide quantifiable measures of the suitability of heat tracing during transient velocities we calculate

252 the maximum error and the root-mean-square error (RMSE) between the modeled and inverted
253 advective thermal velocity and diffusivity data. Finally, we test how well signal processing
254 techniques can distinguish between temperature signal non-stationarity caused by flux transients
255 and other processes by repeating the first set of model simulations with a previously measured
256 and published temperature record [Rau et al., 2010] as the upper boundary.

257 **2.3. Extraction of harmonic amplitudes and phases from temperature records**

258 A prerequisite to the calculation of water flux and thermal diffusivity are temperature time series
259 measured by sensors in at least two different depths of the water-saturated sediment. From these
260 measurements the strongest frequency component, the daily frequency [Stallman, 1965; Hatch et
261 al., 2006; Keery et al., 2007], is commonly extracted. Here, we evaluate the capability and
262 accuracy of the four most commonly used signal processing techniques that offer time-
263 dependent amplitude and phase extraction. To obtain amplitude and phase data from the
264 sinusoidal component embedded in typically noisy field data a transformation of data from the
265 time domain into the frequency domain is needed.

266 **2.3.1. Harmonic peak identification**

267 As a benchmark for the results obtained from different signal processing methods the peak
268 amplitudes and timings were directly identified from the model output. This is only appropriate
269 when the signal consists of a single harmonic frequency as was required by Equations 3-12 and
270 as used for the numerical model. The sampling frequency will limit how accurately peaks
271 (minima and maxima) can be determined. This means that amplitudes and phases may not be
272 optimally detected as any particular minima or maxima may not occur exactly at the sampling
273 time. We apply an algorithm that uses the neighboring values around the peaks to find the exact
274 magnitude and timing with 2^{nd} order polynomial regression. This approach results in a best
275 possible peak time-resolution offering 2 samples per day for peaks. We refer to this approach as
276 "peak picking".

277 **2.3.2. Windowed Fourier Transform (WFT)**

278 The most obvious method is the discrete Fourier transform (DFT) and its computational
279 representation, the fast Fourier transform (FFT). A common approach to obtain frequency
280 information is to apply the FFT to a fixed time window that is shifted along the complete record
281 resulting in the windowed Fourier transform (WFT). This approach was suggested by Keery and
282 Binley [2007] and successfully used by Cuthbert et al. [2011].

WFT offers the advantage of being able to identify signal non-stationarity, as a measure of transient fluxes, in the time domain. However, it is well known that the WFT has a constant frequency resolution due to the fact that the window size used in the time domain defines the resolution in the frequency domain [Oppenheim and Schafer, 1989]. This means that the window size must have an appropriate amount of samples so that the frequency resolution can capture information at 1 cpd. This amounts to window sizes that are multiples of samples per day (one cycle based on daily fluctuations). Further, the minimum window size must be one harmonic cycle in the time domain as otherwise the discrete samples in the frequency domain do not coincide with the desired frequency. While increasing the window size will reduce the artifacts from spectral leakage, this will also diminish the ability to accurately detect the exact timing of changes in the water flux. Since the focus is on determining transient fluxes the minimum window size, a 1 day window with 96 samples (for our sampling interval of 15 min), was used. To maximize the frequency-time information the window was continuously shifted by 1 sample at a time. This approach is equivalent to a moving rectangular window. While different window shapes will change the extracted amplitude-phase relationship, we focus on avoiding any side effects arising from window functions. The amplitude and phase information, given as the length and angle of the complex FFT output, were assigned to the midpoint of the time window. Amplitudes and phases were then used to quantify fluxes and thermal diffusivities with Equations 3-6, 10 and 12.

2.3.3. Zero-phase (forward-backward) filtering

A slightly different amplitude and frequency extraction technique was suggested by Hatch et al. [2006]. Their attempt of recovering the full daily harmonic component in the time domain deployed a windowed filter. The first step is similar to that previously explained for WFT, but then the frequency spectrum is multiplied with a band-pass window centered on 1 cpd to retain the daily frequency and cancel the lower and higher components. This is equivalent to a time-domain convolution of the signal and filter kernel but is often computationally easier. This 1 cpd frequency record is subsequently inverted back to the time domain. Here, the choice of window will have an effect on the spectral leakage, and the *Tukey* window was suggested because it provides an optimization between maintaining the gain for the desired frequency and optimizing the fade of side-band components [Harris, 1978]. The window size (filter order) must be multiples of days to allow accurate sampling of the 1 cpd frequency. Since manipulating the amplitude information in the frequency domain will inevitably also modify the phase information, a forward-backward filter (e.g., Matlab's *filtfilt* function implemented in the Signal

316 Processing Toolbox) must be deployed to allow an exact cancelation of the phase error
317 introduced when filtering in the forward direction only [Hatch et al., 2006].

318 Again, while an increasing window size will result in increasing filter stability it also reduces the
319 temporal resolution (i.e. makes it harder to accurately identify flux transients). A minimum filter
320 order of 384 (= 4 days at 15 min sampling intervals) was determined to result in a stable time-
321 domain output. The filter output in the time domain must undergo "peak picking" before fluxes
322 can be calculated [Hatch et al., 2006].

323 **2.3.4. Continuous Wavelet Transform (CWT)**

324 One significant limitation of the Fourier transform is the Heisenberg–Gabor limit, the
325 relationship between resolution in frequency and time domain [Havin and Jöricke, 1994].
326 However, time-varying amplitude and phase information, as measured for time-varying flux and
327 thermal diffusivity, implies that the signal is non-stationary. The continuous wavelet transform
328 (CWT) appears to be better suited for extracting time-variant frequency domain features from
329 temperature records. Onderka et al. [2013] successfully tested the application of CWT in
330 analytical heat tracing. Pidlisecky and Knight [2011] use CWT to derive infiltration rates from
331 1-D resistivity records. For a useful practical guide to the CWT the interested reader is referred
332 to Torrence and Compo [1998]. Further, Grinsted et al. [2004] offer an excellent practical
333 overview of the wavelet transforms and its application to geophysical time–series.

334 Here, we adopt the same approach as was deployed by Onderka et al. [2013] using the *Morlet*
335 mother wavelet because of its close alignment with the harmonic waveform. In the time domain
336 this wavelet is a superposition of a harmonic and the Gauss function with maximum weight
337 given to the center of the window in the time domain. The wavelet can be stretched or
338 compressed depending on the desired frequency to be analyzed. We used the CWT implemented
339 in Matlab by Erickson [2014].

340 **2.3.5. Dynamic Harmonic Regression (DHR)**

341 Keery et al. [2007] used Dynamic Harmonic Regression (DHR) to extract the diel harmonic
342 from discrete-time temperature records measured at multiple depths in the sediment. DHR was
343 developed by Young et al. [1999] as an extension to Fourier analysis that is particularly suitable
344 for non-stationary signals. The technique is a data based mechanistic approach that features
345 time-variable spectral coefficients that estimate signal amplitude and phase information [Vogt et
346 al., 2010]. DHR is readily implemented in Matlab as the CAPTAIN toolbox [Taylor et al., 2007]
347 and is a state-of-art choice of filter for a non-stationary signal [Young et al., 1999]. For best

compatibility with recent research we implemented DHR in the same way as Keery et al. [2007], Vogt et al. [2010] and in VFLUX [Gordon et al., 2012]. The reader is therefore referred to these papers for further details. Noteworthy is the recommendation for an optimum sampling frequency of 12 samples per day, as over- and under-sampling can cause incorrect signal identification by the DHR algorithm [Gordon et al., 2012].

3. Results and discussion

3.1. Properties of field temperature records and the harmonically-forced analytical solution

As a first point it is vital to consider the characteristics of temperature signals measured in sediments. It is apparent from a number of existing studies that the temperature signal is dominated by the diel and, if the record is long enough, annual frequency [i.e., Hatch et al., 2006; Keery et al., 2007; Wörman et al., 2012]. However, the record typically contains other frequency components that are often referred to as noise. The annual and diel components are controlled by the continuous celestial movements, and thus can be considered harmonics with precisely known cycles (e.g., $P_{diel} = 86,400$ s). More complicated to determine are the "noisy" components which will depend on various natural factors, for example the local climate, site and seasonal specific details (i.e. shading) and sensor noise.

The Fourier Theorem stipulates that a continuous function can be decomposed into an infinite series of individual harmonics with different amplitudes and phases. In practice, temperature measurements are recorded digitally as discrete samples in time. Therefore, the signal can be decomposed into a finite series of harmonics using the Discrete Fourier Transform (DFT). However, it is important to consider that each of the components identified by the DFT is a stationary harmonic, and that the resolution in the time domain will also determine the frequency domain resolution [Oppenheim and Schafer, 1989].

Also noteworthy here is the fact that the differential heat transport equation is of linear nature. This means that the sediment depth response to any temperature signal at the surface is the sum of the individual harmonics that form part of the original signal, but each weighted according to Equation 1 [Goto et al., 2005]. Importantly, the weighting depends on the signal frequency ($f = 1/P$, note P_i in Equation 1) and the water flux, which translates into exponentially damped amplitudes and linearly shifted phases (Figure 1). In other words, the water flux modulates the depth propagation of harmonics. Quantifying the vertical flux from the properties of individual harmonics, i.e. using the amplitude damping and phase shifting, is exactly what heat tracing methods intend to achieve. In essence, the sediment acts as a frequency filter where faster frequencies are damped quicker and slower frequencies propagate further as a function of the vertical flux [Hatch et al., 2006]. This phenomenon has been exploited to calculate thermal diffusivity and a steady-state vertical flux from temperature spectra [Wörman et al., 2012]. It is clear that diel amplitudes and phases cannot simply be selected from unfiltered temperature

385 records, as has been previously done [Fanelli and Lautz, 2008; Lautz, 2010], because the "noise"
386 which consists of inherently different frequencies distorts the diel signal in a depth and flux
387 dependent way. Extraction of amplitude and phase information with signal processing
388 techniques is therefore a crucial component of heat tracing with diurnally forced analytical
389 solutions.

390 In the context of heat tracing it is important to remember that stationary signals require that their
391 statistical properties – here, the features describing a sinusoidal wave – do not change over time
392 [Oppenheim and Schafer, 1989]. When this is considered in relation to Equation 1, it becomes
393 clear that when a hypothetically stationary temperature harmonic (i.e., a temperature sinusoid at
394 the upper boundary) propagates over depth its stationarity is maintained only if the vertical water
395 flux is in steady-state ($v_t = const$ in Equation 1). Importantly, any transients in the water flux
396 (advective thermal velocity $v_t = f(t)$ in Equation 1) will transform a previously stationary
397 harmonic into a non-stationary signal. Figure 2 illustrates this point using a step change in the
398 water flux as a worst case transient for a pure harmonic (a) and actual temperature (b) data
399 obtained from Rau et al. [2010]. In essence, any flux transient, equivalent to a time-change in the
400 advective thermal velocity (v_t) in Equation 1, will influence the stationarity of the temperature-
401 time signal (see also Figure 1) and thus add to any existing non-stationary features already
402 embedded in the temperature signal (Figure 2b).

403 In reality many field studies that develop and apply analytical heat tracing to gain
404 hydrogeological process understanding are interested in the changes in water flux over time. In
405 other words, they rely on the fact that the analytical heat tracing can detect flux transients [e.g.,
406 Hatch et al., 2006; Keery et al., 2007; Lautz et al., 2010; Rau et al., 2010; Swanson and
407 Cardenas, 2010; Vogt et al., 2010; Jensen and Engesgaard, 2011; Munz et al., 2011; McCallum
408 et al., 2012; Luce et al., 2013; McCallum et al., 2014; Tonina et al., 2014; Gariglio et al., 2014].
409 Here, we test whether flux transients can be quantified using analytical methods and determine
410 their behavior when the temperature signal becomes non-stationary caused by transient fluxes.
411 From a signal processing perspective it is useful to investigate how accurately the onset of
412 sudden signal non-stationarity can be delineated and attributed to a cause, such as changes in the
413 water flux implicitly expressed in the temperature records.

3.2. System response to sudden water flux transients

It is important to understand the thermal modulation of transient fluxes before proceeding with the analysis of signal amplitude and phase extraction methods, and their subsequent impact on the quantification of thermal diffusivities or sediment scour/deposition and the temporal fluxes. This provides the foundation for a quantitative assessment of the possible artifacts that signal processing imposes on the physical processes contained within temperature harmonics.

How long does it take for a harmonic temperature signal to return to stationarity when affected by a sudden change in flux, e.g. a step change? Figure 3a shows the sediment thermal response to sudden advective thermal velocity transients. This is defined as the difference between the numerically modeled temperature response to a velocity step change and the stationary temperature signals that were calculated with Equations 1-2 for the two different steady-state velocities that the step consists of. The thermal response is shown for two different depths and a minimum, average and maximum thermal diffusivity (as was used by Shanafield et al. [2011] and McCallum et al. [2012]). After an initial temperature jump (sharp non-stationarity) caused by the velocity step it is clear that the underlying thermal response resembles the characteristic exponential relaxation described by the generic equation $\exp(-t/\tau)$, where τ is the response time [T]. The magnitude of the temperature non-stationarity induced by the velocity step decreases from approx. 2.3 °C to 0.2 °C (for a boundary amplitude of 3 °C) with increasing thermal diffusivity (Figure 3a). The relaxation time τ for $D_{avg} = 0.075$ m^2/d is approx. 0.15 days, but this depends on the speed of propagation (velocity magnitude and depth of measurement) and the sediment thermal diffusivity. Figure 3a reveals that the minimum thermal diffusivity causes the largest initial temperature jump but also the shortest thermal response time (~0.04 days for a spacing of 0.1 m).

Not surprisingly, the sediment thermal response will also depend on the timing of the velocity transient in relation to the phase of the upper harmonic temperature boundary. Figure 3b shows an example of the velocity step change with the onset occurring at 8 different times shifted by 0.125 days ($\pi/4$ for $f = 1$ cpd). Again, the sediment thermal response at depth was calculated as the difference between the temperature output from the numerical model and the analytical solution. Interestingly, the magnitude of the thermal response ranges between ~0.1 °C and 1.4 °C for the step at 0.125 d and 0.375 d, respectively, and with shape of the sediment thermal response suggesting a more complex function compared to just an exponential relaxation. Nevertheless, the perturbation decays over time as expected.

In summary, a water flux step change causes a sudden propagation of non-stationarity in the temperature signal over depth followed by gradual return to stationarity over time. This is due to the previously stationary temperature-depth harmonic being moved downwards or upwards by the sudden change in water flux before stationarity is reached again. For the velocity used in this example and for realistic thermal diffusivities ($0.02 < D < 0.13$ m^2/d) the sediment response time is $0.04 < \tau < 0.24$ days. Importantly, it is evident that the temperature non-stationarity caused by a worst-case transient velocity (step change) diminishes within one harmonic cycle (1 day).

3.3. How do different signal extraction methods perform when the signal is non-stationary?

Figure 2b suggests that the temperature non-stationarity caused by a transient water flux is superimposed on temperature signal non-stationarities caused by other factors (see earlier discussion). While the importance of correctly extracting amplitudes and phases was established earlier, it is vital to reveal how different signal extraction techniques respond to non-stationarity caused by only the transient water flux, since these transients are of main interest. Hatch et al. [2006] discussed the possible impact of signal filter edge effects on the fluxes and suggested that the effect of filtering should be further investigated. While different authors have used various different signal processing techniques [Hatch et al., 2006; Keery et al., 2007; Cuthbert et al., 2011; Onderka et al., 2013], their impact on the flux results have mostly been assumed negligible, and were neither comprehensively investigated nor quantified.

Here, we raise the question: How accurate are different signal processing techniques in delineating non-stationary harmonic features (e.g. amplitudes and phases) caused by transient fluxes when they are buried in a "noisy" signal? This can be answered by comparing the response of signal extraction techniques to a sudden non-stationarity. Figure 4 illustrates the response of four different signal processing techniques (WFT, filtfilt, CWT and DHR; see methods section for details) to the non-stationarity of an otherwise harmonic temperature signal caused by a step change in advective thermal velocity. Figures 4a, 4c, 4e, 4g show the extracted amplitudes and 4b, 4d, 4f, 4h the phases at different depths with time relative to the non-stationarity. Since both amplitude and phase are combined to invert the vertical velocity and thermal diffusivity (see Equations 7-12) it is essential to inspect both separately.

Figure 4 demonstrates the following features:

- The four signal processing techniques demonstrate different responses to non-stationarity

- While the extracted signal amplitudes are generally smooth, the phase data can exhibit significant artifacts, e.g. oscillations (Figure 4b,d,f,h)
- The response to signal non-stationarity is an erroneous temporal spreading ("smearing") over time, with both the amplitude and phase responding before the actual velocity transient has occurred
- Significant "smearing" occurs for a minimum of 1 cycle for WFT (Figure 4a,b), and maximum time of ~3 cycles for filtfilt (Figure 4c,d)
- The WFT methods shows strong oscillations in particular for phase data where the signal to noise ratio is low, e.g. for the deepest observation points (Figure 4b)

In general, the above observations highlight that signal processing can strongly impact the quantification of vertical fluxes and thermal diffusivities during transient changes.

3.4. Quantification of transient fluxes and thermal diffusivities

The previously presented amplitude and phase data (Figure 4) were used to derive amplitude ratios (Equation 3) and phase shifts (Equation 4) based on two observation points located at different depths. Then, the velocities and thermal diffusivities were quantified from Equations 7-12 and compared with those used as input to the numerical model. This was done with amplitude and phase data extracted using all four signal processing techniques (Figure 4). Figure 5 summarizes the vertical velocities (a, c, e, g) and thermal diffusivities (b, d, f, h) for different velocity step changes, 0 to -1 m/d (a & b), 0 to 1 m/d (c & d), reversal from -1 m/d to 1 m/d (e & f) and reversal from 1 m/d to -1 m/d (g & h). As a best-case benchmark the results from picking amplitudes and phases straight from the simulated temperature data (which is possible in this case since a sinusoidal temperature boundary is used), are also shown. We emphasize that this approach presents the best possible time resolution that can be achieved from methods that rely on a harmonic signal, as a sinusoid only has 2 features per cycle (amplitudes and phases at maximum and minimum).

Figure 5 shows significant artifacts in vertical velocities and thermal diffusivities that stem from quantifying the heat tracing derived velocity over a step change in the modeled water velocity. Best results are achieved when peak picking is applied to unfiltered harmonic temperature data (red squares in Figure 5) showing only a small deviation from the modeled velocity. The errors between modeled and inverted velocity are caused by the streambed's non-stationary thermal response, as was discussed earlier (Section 3.2, Figure 3). However, this approach can only be

used when the temperature signal is a pure harmonic (stationary) and must not be applied to noisy real-field measurements.

Being deduced from the previously shown amplitude and phase data (Figure 4) the velocity and diffusivity results are also "smeared" across ~4-5 cycles, approximately centered at the time at which the transient velocity occurred (Figure 5). It is noteworthy that for downward velocity steps the thermal diffusivity is overestimated, and it is underestimated for upward velocity steps. Note that sensor spacing (Equation 11) is prone to the same anomaly because it originates from reformulating the thermal diffusivity (Equation 10). Figures 6 and 7 show the same calculation for different velocity step sizes in both directions and found that the response becomes increasingly smeared and delayed for large velocity steps. Interestingly, the results in Figures 5, 6 and 7 also indicate that for velocity steps up to ±1 m/d the "smearing" is independent of either the velocity step magnitude or direction, even for velocity reversals. Further, results show that for velocity transients exceeding -5 m/d (Figure 6) and 2 m/d (Figure 7) the response shifts forward in time and the error between modeled and inverted advective velocity increases significantly.

These results demonstrate that signal processing techniques, and not the assumption of steady-state flux inherent to the analytical solution (Equation 1), is the culprit responsible for inaccurate detection of transient fluxes quantified from harmonically forced analytical solutions. This is due to the uncertainty principle (Heisenberg-Gabor limit) based on fixed resolution in both time and frequency domain inherent to any signal filtering that relies on the Fourier transform [Havin and Jöricke, 1994].

While the scenarios presented in Figures 5-7 resemble a worst case caused by highly transient hydrographs (e.g. flash floods, dam releases), streams that are dominated by snowmelt typically experience slower flux transients. Figure 8 shows the response of heat tracing to different rates of velocity change (an analogue of the hydrograph slope assuming no change of hydraulic conductivity over time) modeled as a linear increase of the advective thermal velocity from 0 to -1 m/d within 0.5, 1, 2 and 4 days. A summary of the match between modeled and inverted advective thermal velocities and diffusivities can be found in Tables 1 and 2, respectively, for the four different filtering methods and the four different rates of velocity change (Figure 8) as well as the step change (first row in Figure 5). Here, it is interesting to note that the velocities inverted without applying any signal processing methods directly from the temperature amplitudes and phases (red markers) in all cases closely resemble the actual velocities used to drive the numerical model (Figure 8 first column, RMSE < 0.031 ºC in all cases). In contrast

542 inverted thermal diffusivities (or sensor spacing) are more sensitive to flux transients, with
543 values generally underestimated and with decreasing errors for a decreasing rate of velocity
544 change (Figure 8 second column). The time decay of the error is in agreement with the
545 streambed thermal response evaluated in Figure 3.

546 Figure 8 further illustrates the capability of the different signal processing methods to delineate
547 different degrees of signal non-stationarity. As expected, the less transient the better the response
548 of signal processing methods, indicated by the degree of matching between modeled and
549 inverted velocity (decreasing RMSE in Table 1). It is apparent that DHR is the overall best
550 performing (most time-variant) method with inverted and modeled velocities matching the
551 closest (smallest RMSE in Tables 1 and 2). By contrast, CWT shows the slowest response to
552 velocity transients (highest RMSE in Tables 1 and 2). Interestingly, thermal diffusivities inverted
553 after applying the signal processing methods are consistently overestimated during the velocity
554 transient. Further, it is noteworthy that there remains a significant error in the inverted velocities
555 (max. 0.06 m/d for DHR) and diffusivities for a velocity ramp that spans 4 harmonic cycles. This
556 proves that heat tracing results are increasingly affected by the signal processing methods under
557 increasing transient advective velocities (see RMSE values in Tables 1 and 2). Sudden flux
558 transient can cause errors of up to 57 % in velocity (Table 1) and 37 % in thermal diffusivity
559 (Table 2) estimates even when DHR, the most time-variant spectral filter, is used. Inaccuracies
560 in the inverted results persist for up to ±2 days around the occurrence of sudden flux transients
561 (Figures 5 and 8). The mildest case of velocity transient studied here (-1 m/d velocity change in
562 4 days: $dv/dt = 0.25$ m/d^2) introduces an error of ~6 % in velocity (Table 1) and ~4 % in
563 thermal diffusivity (Table 2) with inaccuracies during ±1 days of the start and end of the velocity
564 change (Figures 8 and first row in Figure 5). These errors are larger for all other signal
565 processing methods and rates of velocity change studied.

566 McCallum et al. [2012] have reported spurious thermal diffusivities in their field investigation
567 during highly transient flow conditions, e.g. dam releases and floods. Further, they found that
568 water flux calculated by heat tracing reacted before the change in hydraulic gradients. Both
569 observations are consistent with the erroneous delineation of transient fluxes caused by signal
570 processing as illustrated in this paper (see Figures 5 and 6). It has previously been suggested that
571 sub-cycle resolution for vertical fluxes can be obtained [Lautz, 2012]. Here, we demonstrate
572 that, while signal processing techniques offer sub-cycle resolution values for amplitudes and
573 phases, the smoothing of the inverted fluxes across sudden transients (and oscillations in the case
574 of phase data) may not resemble the actual transient flux. It is therefore not recommended to

trust flux and thermal diffusivity or sediment scour/deposition results during times when fluxes are expected to be transient (e.g. floods). This suggests that hydraulic head data should be interpreted together with temperature data in order to assess transient conditions; otherwise the use of heat tracing based on harmonic signals becomes untrustworthy.

The above discussion raises the question as to which signal processing technique performs best under transient flux conditions. Figure 5 suggests that there is no simple answer, as there appears to be a trade-off between the distortion of the magnitude and the duration of the flux and diffusivity estimates. The most suitable approach will depend on the individual circumstances and whether the focus lies on estimating the magnitude or timing of transient fluxes.

3.5. Biased process estimates caused by a non-stationary temperature boundary

While the previous discussion revealed that signal processing techniques hamper the accurate time-resolution of quantified fluxes and thermal diffusivities or sediment scour/deposition when the water flux is transient, the influence of non-stationarity in the field temperature records has so far been neglected but must also be considered. Rau et al. [2010] measured the temperatures at the bottom of the stream column and at several depths within the streambed sediment with a sensor spacing of 0.15 m at 3 different horizontal locations within a small perennial stream in Australia over a 3-month period in 2007. Here, we use a 30-day subset of the uppermost temperature data from location C (see Rau et al. [2010]) as a real-field boundary condition for our numerical model. Figure 9a shows the multi-level temperature time series obtained from numerical modeling using a velocity step change and the measured surface water temperature as the boundary condition [Rau et al. 2010]. Here, the non-stationarity is present in the system due to both natural causes (e.g. weather changes, site specific shading, sensor noise, see 3.1 earlier) and water flux imposed by the flux step. The challenge for the accurate detection of amplitudes and phases is to maximize the extracted signal induced by the change in the water flux and to minimize the "noise" with frequencies other than diel in the forcing temperature data.

Figures 9b and 9c show vertical velocities and thermal diffusivities quantified with Equations 10 and 12 after applying the different signal processing techniques outlined in the methods section. The results clearly show that general temperature non-stationarity significantly 'leaks' into the velocity results. The WFT is revealed as the worst performing technique with apparent velocity variations of similar magnitude to the actual velocity step that is to be identified. This is due to the shortness of the 1-day window selected to maximize the detection of the timing of the velocity transients. Increasing the window would increase the method's accuracy during steady

607 velocity periods, but at the expense of reducing its ability to accurately delineate the step change.
608 The technique with best performing amplitudes and phase extraction is the zero-phase forward-
609 backward filter (*filtfilt* in Matlab), originally proposed by Hatch et al. [2006]. However, this
610 method still smooths the velocity transient (Figure 9b), and produces an apparent jump in
611 thermal diffusivity (Figure 9c), caused by the window length. By contrast DHR, which has been
612 attributed with robust detection of harmonics embedded in non-stationary signals [Vogt et al.,
613 2010; Gordon et al., 2012], exhibits significant noise in our test (Figures 7b and 7c). Our results
614 confirm what McCallum et al. [2012] had observed in their field application, mainly that heat
615 tracing results should not be trusted during times when the flux is expected to be transient. We
616 suggest that thermal diffusivity jumps in field data indicate times when the vertical flux is highly
617 transient or when erosion-depositional processes occur. However, as both would occur during
618 transient conditions it would be difficult to disentangle real changes in sensor spacing (as a
619 proxy for scour/depositional processes) from anomalies induced by transient velocities (Figures
620 5-8).

621 Figure 9 also demonstrates that there is a lower limit to the detection of velocity changes. This
622 limit depends on the signal-to-noise ratio, the ratio between temperature signal non-stationarity
623 caused by the transient water flux and other sources of non-stationarity. Fourier based signal
624 processing methods are prone to leakage between different frequencies. Leakage can obscure the
625 harmonic signal of interest, depends on the filter parameters and is difficult to quantify. The
626 forcing temperature may contain many simultaneous sources of non-stationarity with different
627 frequencies and magnitudes buried in the diel temperature records (e.g. caused by the local
628 climate, seasonal shading, surface flow, etc.). Therefore, the detectability of transient flux
629 magnitudes will depend on the strength of non-stationarity from other sources. In some cases it
630 may become impossible to disentangle the diel frequency from other sources of non-stationarity.
631 Our results illustrate that while signal processing is mandatory to extract harmonic amplitude
632 and phases its limited ability to deal with signal non-stationarity thwarts the accurate delineation
633 of transient fluxes and thermal diffusivities or sediment scour/deposition.

634 McCallum et al. [2012] observed that the thermal diffusivities calculated from heat tracing can
635 temporarily exceed any physically plausible limits. Further, they warned that this could be due to
636 violated boundary conditions for the analytical solution. Here, we show that the apparent
637 "jumps" in thermal diffusivity originate from signal processing artifacts caused by transient
638 water fluxes that impose sudden non-stationarity on the underlying temperature signal. These

signal features are too fast for methods that make use of Fourier based time-frequency transformation and are thus incorrectly delineated.

In a different study, Luce et al. [2013] proposed that streambed scouring could be inferred from quantifications of apparent variation in sensor spacing Δz, rather than thermal diffusivity. Tonina et al. [2014] tested the quantification of time-variant scour and deposition with analytical heat tracing in combination with DHR and Equations 9-11. While they tested the method's capability by manually changing the amount of sediment above the buried temperature sensor during times when the flux was relatively steady, naturally occurring sediment movement typically occurs when the stream discharge is high. This implies transient stream discharge conditions which are also the main driver for transient vertical fluxes. Gariglio et al. [2014] attributed highly variable thermal diffusivities with values exceeding physically plausible limits, as calculated during times of transient river discharge using DHR, to sediment scour/deposition. We point out that quantifying naturally occurring sediment movement, such as scour and depositional processes, using analytical heat tracing may be a challenging proposition. This is because a) the derivation for sensor spacing is the same but rearranged equation as that for thermal diffusivity (Equations 10 and 11) and results are prone to artifacts as illustrated earlier, and b) the natural example presented in Luce et al. [2013] suggests that the water flux was transient as indicated by the fluctuating river discharge data. Flux and diffusivity artifacts arising from signal non-stationarity, which are to be expected during transient discharge conditions when sediment movement likely occurs simultaneously, could thus easily be mistaken for scour/depositional processes. We demonstrate that heat tracing based on harmonic signals becomes increasingly unsuitable to quantify vertical fluxes, thermal diffusivities or sediment scour/deposition from temperature data under increasingly transient flow conditions.

Sediment temperature data reported in the literature and acquired during highly transient hydraulic events (e.g. floods) at the system boundary exhibit high non-stationarity in regards to harmonic components (e.g. see Barlow et al. [2009]; Mutiti and Levy [2010]). We expect that the risk of leakage due to signal time-frequency transformation, and associated impact on amplitude and phase data, will contribute considerable uncertainty to the delineation of transient fluxes, thermal diffusivities or sediment scour/deposition. Furthermore, flux transients often occur on time scales less than one harmonic cycle (e.g. duration of flood peak, dam releases or the onset or cessation of near-stream groundwater pumping). Consequently, to quantify highly transient fluxes and thermal diffusivity or sediment scour/deposition under such conditions we recommend that numerical approaches be deployed [e.g. Holzbecher, 2005; Voytek et al., 2013],

672 or that methods based on signal processing techniques offering improved delineation of transient
673 processes from frequency-domain data are deployed or developed.

4. Conclusion

A thorough analysis of Stallman's [1965] analytical solution reveals that changes in the vertical water flux induce non-stationarity in the temperature signal during its propagation. The severity of non-stationarity depends on the magnitude of the flux transient. A simulated worst case water velocity transient (step change from 0 to -1 m/d with harmonic amplitude of 3 ºC) triggers an abrupt transition to non-stationarity in the sediment temperature signal. The response (difference between modeled temperature and analytical solution assuming steady-state velocity) depends on the thermal diffusivity and the onset of the velocity step change relative to the phase of the harmonic temperature boundary. The maximum response is ~2.3 ºC and return to stationarity occurs within 1 harmonic cycle (= 1 day) for physically plausible sediment thermal diffusivities in the range of 0.02-0.13 m^2/d.

Inverting transient vertical fluxes and thermal diffusivities from temperature records using analytical heat tracing relies either on the transformation of the signal from time to frequency domain, or extraction of time-variable amplitude and phase information of a fixed-frequency harmonic. Both are only possible with signal processing techniques. We benchmarked the ability of four commonly used signal processing methods (windowed Fourier transform (WFT), forward-backward zero phase filter (filtfilt), continuous wavelet transform (CWT) and dynamic harmonic regression (DHR)) to delineate signal non-stationarity implicit in the temperature-time signal. This was done by numerically simulating the transient advective thermal velocity with a harmonic temperature boundary and comparing the known to the inverted velocities obtained by the signal processing and the analytical solution. All the signal processing techniques were shown to offer poor time-domain resolution of frequency-domain features, and to erroneously spread amplitude and phase information across up to approx. 4 harmonic cycles (4 days). There is a technique and parameter dependent trade-off between magnitude and duration of the response to abrupt signal non-stationarity.

In essence, our analysis shows that the ability to accurately resolve flux transients with analytical heat tracing is currently limited by the signal processing, rather than the assumption of steady-state flow inherent to Stallman's [1965] analytical solution. This is because local signal stationarity is assumed for each extracted amplitude and/or phase value. The signal processing response appears to be independent of the advective thermal velocity step size, including reversal, for steps smaller than ±1 m/d. The match between modeled and inverted velocities improves with decreasing rates of velocity change. Implications on heat tracing are that: a) a sudden sharp transient in apparent velocity appears smoothed and earlier than the hydraulic

driver, and b) an apparent thermal diffusivity overshoot (undershoot) for a downward (upward) velocity change with values that can exceed physically plausible limits. The latter is caused by signal processing methods introducing phase artifacts originating from response to signal non-stationarity. While the thermal diffusivity anomaly can be used as an indication of a flux transient (including direction), the quantified flux and diffusivity values or sensor spacing (sediment scour/deposition) should not be trusted during that time.

Real-world temperature records contain non-stationarities caused by a range of different superimposed factors, such as abrupt hydrologic or meteoric changes, or anthropogenic disturbances. We applied the commonly used heat tracing techniques to numerically simulated streambed temperatures with the model driven by previously presented surface water temperature data [Rau et al., 2010] as the upper boundary. Inversion of fluxes and thermal diffusivities from the simulated temperatures reveals that, besides the erroneous temporal spreading of the flux transient (time-smearing), there are anomalies in the diffusivity results that originate from the signal processing techniques. The forward-backward zero-phase filter was identified as the best-performing amplitude and phase extraction method causing the least artifacts, but limited to producing 2 flux results per day.

Our results have significant implications for the practical application of inverting water fluxes, thermal diffusivities or sensor spacing (scour/deposition) from temperature data using increasingly popular methods that are based on harmonically forced analytical solutions. While these techniques are useful to estimate fluxes during times when hydraulic drivers indicate steady-state conditions, attention must be paid during transient conditions. This suggests that, when highly transient fluxes are to be calculated from temperature records, hydraulic heads should be monitored alongside temperature data, and that either numerical methods or new signal processing methods extracting features in the time domain must be applied. Besides the implications for heat tracing in near-surface water systems, our results point out that the response of signal processing techniques to non-stationary data must be carefully considered when time-varying physical processes are inferred from frequency-domain information in other geophysical datasets.

Acknowledgements

Funding was provided by the Gary Johnston fund that started the Chair of Water Management at UNSW Australia. Mark Cuthbert was supported by Marie Curie Research Fellowship funding from the European Community's Seventh Framework Programme [FP7/2007-2013] under grant agreement n.299091. Landon Halloran was supported by a UNSW School of Civil and Environmental Engineering scholarship and a Canadian "Fonds de Recherche du Québec - Nature et Technologies" (dossier: 173538). The data for this paper are available by contacting the corresponding author. We thank Giovanni Coco (editor) for handling our manuscript and Jason Kean (associate editor) for very comprehensive and helpful feedback. Further, we are grateful to Jim Constantz and 2 anonymous reviewers for their constructive suggestions that have significantly strengthened this work.

References

Anderson, M. P. (2005), Heat as a Ground Water Tracer, *Ground Water*, *43*(6), 951-968, doi: 10.1111/j.1745-6584.2005.00052.x.

Barlow, J. R. B., and R. H. Coupe (2009), Use of heat to estimate streambed fluxes during extreme hydrologic events, *Water Resources Research*, *45*, W01403, doi: 10.1029/2007WR006121.

Best, A. I., C. McCann, and J. Sothcott (1994), The relationships between the velocities, attenuations and petrophysical properties of reservoir sedimentary rocks1, *Geophysical Prospecting*, *42*(2), 151-178, doi: 10.1111/j.1365-2478.1994.tb00204.x.

Constantz, J. (2008), Heat as a tracer to determine streambed water exchanges, *Water Resources Research*, *44*, -, doi: 10.1029/2008WR006996.

COMSOL (2014), COMSOL Multiphysics Version 5, COMSOL Inc., Burlington, MA, USA.

Cuthbert, M. O. (2010), An improved time series approach for estimating groundwater recharge from groundwater level fluctuations, *Water Resources Research*, *46*(9), W09515, doi: 10.1029/2009WR008572.

Cuthbert, M. O., and R. Mackay (2013), Impacts of nonuniform flow on estimates of vertical streambed flux, *Water Resources Research*, *49*(1), 19-28, doi: 10.1029/2011WR011587.

Cuthbert, M. O., R. Mackay, V. Durand, M.-F. Aller, R. B. Greswell, and M. O. Rivett (2010), Impacts of river bed gas on the hydraulic and thermal dynamics of the hyporheic zone, *Advances in Water Resources*, *33*, 1347-1358, doi: 10.1016/j.advwatres.2010.09.014.

766 Erickson, J. (2014), Continuous wavelet transform and inverse, Matlab Central,
767 <http://www.mathworks.com/matlabcentral/fileexchange/20821-continuous-wavelet-transform-
768 and-inverse>, updated: 14/10/2014, accessed: Jan 2015.

769 Fanelli, R. M., and L. K. Lautz (2008), Patterns of water, heat, and solute flux through
770 streambeds around small dams., *Ground Water*, *46*, 671-687, doi: 10.1111/j.1745-
771 6584.2008.00461.x.

772 Gordon, R. P., L. K. Lautz, M. A. Briggs, and J. M. McKenzie (2012), Automated calculation of
773 vertical pore-water flux from field temperature time series using the VFLUX method and
774 computer program, *Journal of Hydrology*, *420-421*, 142-158, doi:
775 10.1016/j.jhydrol.2011.11.053.

776 Goto, S., M. Yamano, and M. Kinoshita (2005), Thermal response of sediment with vertical
777 fluid flow to periodic temperature variation at the surface, *J Geophys Res-Sol Ea*, *110*, B01106,
778 doi: 10.1029/2004JB003419.

779 Gariglio, F. P., D. Tonina, and C. H. Luce (2013), Spatiotemporal variability of hyporheic
780 exchange through a pool-riffle-pool sequence, *Water Resources Research*, *49*(11), 7185-7204,
781 doi: 10.1002/wrcr.20419.

782 Harris, F. J. (1978), On the use of windows for harmonic analysis with the discrete Fourier
783 transform, *Proceedings of the IEEE*, *66*(1), 51-83, doi: 10.1109/PROC.1978.10837.

784 Hatch, C. E., A. T. Fisher, J. S. Revenaugh, J. Constantz, and C. Ruehl (2006), Quantifying
785 surface water–groundwater interactions using time series analysis of streambed thermal records:
786 Method development, *Water Resources Research*, *42*, W10410, doi: 10.1029/2005WR004787.

787 Havin, V., and B. Jöricke (1994), *The uncertainty principle in harmonic analysis*, Springer.

788 Holzbecher, E. (2005), Inversion of temperature time series from near-surface porous sediments,
789 *Journal of Geophysics and Engineering*, *2*, 343-348, doi: 10.1088/1742-2132/2/4/S07.

790 Irvine, D. J., R. H. Cranswick, C. T. Simmons, M. A. Shanafield, and L. K. Lautz (2015), The
791 effect of streambed heterogeneity on groundwater-surface water exchange fluxes inferred from
792 temperature time series, *Water Resources Research*, n/a-n/a, doi: 10.1002/2014WR015769.

793 Jensen, J. K., and P. Engesgaard (2011), Nonuniform Groundwater Discharge across a
794 Streambed: Heat as a Tracer, *Vadose Zone J*, *10*, 98, doi: 10.2136/vzj2010.0005.

795 Keery, J. S., and A. Binley (2007), Temperature measurements for determining groundwater–
796 surface water fluxes, *Rep. Science Report SC030155/SR9*, Environment Agency & Lancaster
797 University, Bristol, UK.

798 Keery, J., A. Binley, N. Crook, and J. W. N. Smith (2007), Temporal and spatial variability of
799 groundwater–surface water fluxes: Development and application of an analytical method using
800 temperature time series, *Journal of Hydrology*, *336*, 1-16, doi: 10.1016/j.jhydrol.2006.12.003.

801 Lautz, L. K. (2010), Impacts of nonideal field conditions on vertical water velocity estimates
802 from streambed temperature time series, *Water Resources Research*, *46*, W01509, doi:
803 10.1029/2009WR007917.

804 Lautz, L. K. (2012), Observing temporal patterns of vertical flux through streambed sediments
805 using time-series analysis of temperature records, *Journal of Hydrology*, *464–465*, 199–215, doi:
806 10.1016/j.jhydrol.2012.07.006.

807 Luce, C. H., D. Tonina, F. Gariglio, and R. Applebee (2013), Solutions for the diurnally forced
808 advection-diffusion equation to estimate bulk fluid velocity and diffusivity in streambeds from
809 temperature time series, *Water Resources Research*, *49*(1), 488-506, doi:
810 10.1029/2012WR012380.

811 McCallum, A. M., M. S. Andersen, G. C. Rau, and R. I. Acworth (2012), A 1D analytical
812 method for estimating surface water groundwater interactions and effective thermal diffusivity
813 using temperature time series, *Water Resources Research*, *48*, W11532.

814 McCallum, A. M., M. S. Andersen, G. C. Rau, J. R. Larsen, and R. I. Acworth (2014), River-
815 aquifer interactions in a semiarid environment investigated using point and reach measurements,
816 *Water Resources Research*, *50*(4), 2815-2829, doi: 10.1002/2012WR012922.

817 Munz, M., S. E. Oswald, and C. Schmidt (2011), Sand box experiments to evaluate the influence
818 of subsurface temperature probe design on temperature based water flux calculation, *Hydrology*
819 *and Earth System Sciences Discussions*, *8*, 6155-6197, doi: 10.5194/hessd-8-6155-2011.

820 Mutiti, S., and J. Levy (2010), Using temperature modeling to investigate the temporal
821 variability of riverbed hydraulic conductivity during storm events, *Journal of Hydrology*, *388*,
822 321-334, doi: 10.1016/j.jhydrol.2010.05.011.

823 Onderka, M., S. Banzhaf, T. Scheytt, and A. Krein (2013), Seepage velocities derived from
824 thermal records using wavelet analysis, *Journal of Hydrology*, *479*(0), 64-74, doi:
825 10.1016/j.jhydrol.2012.11.022.

826 Oppenheim, A. V., R. W. Schafer, and J. R. Buck (1989), *Discrete-time signal processing*,
827 Prentice-hall Englewood Cliffs.

828 Pidlisecky, A., and R. Knight (2011), The Use of Wavelet Analysis to Derive Infiltration Rates
829 from Time-Lapse One-Dimensional Resistivity Records, *Vadose Zone*, *10*(2), 697-705, doi:
830 10.2136/vzj2010.0049.

831 Rau, G. C., M. S. Andersen, and R. I. Acworth (2012a), Experimental investigation of the
832 thermal dispersivity term and its significance in the heat transport equation for flow in
833 sediments, *Water Resources Research*, *48*, W03511, doi: 10.1029/2011WR011038.

834 Rau, G. C., M. S. Andersen, and R. I. Acworth (2012b), Experimental investigation of the
835 thermal time-series method for surface water-groundwater interactions, *Water Resources*
836 *Research*, *48*, W03530, doi: 10.1029/2011WR011560.

837 Rau, G. C., M. S. Andersen, A. M. McCallum, and R. I. Acworth (2010), Analytical methods
838 that use natural heat as a tracer to quantify surface water–groundwater exchange, evaluated using
839 field temperature records, *Hydrogeol J*, *18*, 1093-1110, doi: 10.1007/s10040-010-0586-0.

840 Roshan, H., G. C. Rau, M. S. Andersen, and I. R. Acworth (2012), Use of heat as tracer to
841 quantify vertical streambed flow in a two-dimensional flow field, *Water Resources Research*,
842 *48*(10), W10508, doi: 10.1029/2012WR011918.

843 Shanafield, M., C. Hatch, and G. Pohll (2011), Uncertainty in thermal time series analysis
844 estimates of streambed water flux, *Water Resources Research*, *47*, W03504, doi:
845 10.1029/2010WR009574.

846 Soto-López, C. D., T. Meixner, and T. P. A. Ferré (2011), Effects of measurement resolution on
847 the analysis of temperature time series for stream-aquifer flux estimation, *Water Resources*
848 *Research*, *47*, W12602, doi: 10.1029/2011WR010834.

849 Stallman, R. W. (1965), Steady One-Dimensional Fluid Flow in a Semi-Infinite Porous Medium
850 with Sinusoidal Surface Temperature, *J Geophys Res*, *70*, 2821-2827, doi:
851 10.1029/JZ070i012p02821.

852 Suzuki, S. (1960), Percolation Measurements Based on Heat Flow Through Soil with Special
853 Reference to Paddy Fields, *J Geophys Res*, *65*, 2883, doi: 10.1029/JZ065i009p02883.

854 Swanson, T. E., and M. B. Cardenas (2010), Diel heat transport within the hyporheic zone of a
855 pool-riffle-pool sequence of a losing stream and evaluation of models for fluid flux estimation
856 using heat, *Limnol. Oceanogr.*, *55*, 1741-1754, doi: 10.4319/lo.2010.55.4.1741.

857 Swanson, T. E., and M. B. Cardenas (2011), Ex-Stream: A MATLAB program for calculating
858 fluid flux through sediment–water interfaces based on steady and transient temperature profiles,
859 *Computers & Geosciences*, *37*, 1664-1669, doi: 10.1016/j.cageo.2010.12.001.

860 Tonina, D., C. Luce, and F. Gariglio (2014), Quantifying streambed deposition and scour from
861 stream and hyporheic water temperature time series, *Water Resources Research*, *50*(1), 287-292,
862 doi: 10.1002/2013WR014567.

863 Torrence, C., and G. P. Compo (1998), A practical guide to wavelet analysis, *Bulletin of the*
864 *American Meteorological society*, *79*(1), 61-78.

865 Vogt, T., P. Schneider, L. Hahn-Woernle, and O. A. Cirpka (2010), Estimation of seepage rates
866 in a losing stream by means of fiber-optic high-resolution vertical temperature profiling, *Journal*
867 *of Hydrology*, *380*, 154-164, doi: 10.1016/j.jhydrol.2009.10.033.

868 Voytek, E. B., A. Drenkelfuss, F. D. Day-Lewis, R. Healy, J. W. Lane, and D. Werkema (2013),
869 1DTempPro: Analyzing Temperature Profiles for Groundwater/Surface-water Exchange,
870 *Groundwater*, doi: 10.1111/gwat.12051.

871 Wörman, A., J. Riml, N. Schmadel, B. T. Neilson, A. Bottacin-Busolin, and J. E. Heavilin
872 (2012), Spectral scaling of heat fluxes in streambed sediments, *Geophysical Research Letters*,
873 *39*(23), L23402, doi: 10.1029/2012GL053922.

874 Wu, W., M. A. Geller, and R. E. Dickinson (2002), A case study for land model evaluation:
875 Simulation of soil moisture amplitude damping and phase shift, *Journal of Geophysical*
876 *Research: Atmospheres*, *107*(D24), 4793, doi: 10.1029/2001JD001405.

877 Young, P. C., D. J. Pedregal, and W. Tych (1999), Dynamic harmonic regression, *Journal of*
878 *Forecasting*, *18*, 369-394, doi: 10.1002/(SICI)1099-131X(199911)18:6<369::AID-
879 FOR748>3.0.CO;2-K.

880 **Figure captions**

881 Figure 1: Damping of amplitude (a) and shifting of phase (b) with depth for a sinusoid with
882 frequency of 1 cpd calculated using Stallman's [1965] analytical solution. Shaded areas
883 represent ranges based on effective thermal diffusivities $D_{min} = 0.02\ m^2/d$, $D_{avg} = 0.075\ m^2/d$
884 and $D_{max} = 0.13\ m^2/d$ as reported in the literature [Shanafield et al., 2011; McCallum et al.,
885 2012]. Dashed horizontal lines show the depths at which temperature time-series were output
886 from the numerical model.

887 Figure 2: a) An example of multi-level temperature harmonics in response to a step change in
888 vertical water velocity as output from the numerical model. Here, Δz refers to sensor spacing of
889 0, 0.05, 0.2 and 0.4 m from the top of the sediment plotted with increasing intensity of black
890 color. The data serves to illustrate that a stationary harmonic is transformed into a non-stationary
891 harmonic through a transient in the vertical water velocity. b) Modeled multi-level temperature
892 data using real sediment temperature measurements at the streambed surface (from Rau et al.
893 [2010]) as a boundary for the same velocity as in a).

894 Figure 3: a) The thermal response to a transient water velocity: The temperature difference
895 between numerically modeled and analytically calculated harmonics due to a step change in
896 velocity from 0 to -1 m/d for $D_{min} = 0.02\ m^2/d$, $D_{avg} = 0.075\ m^2/d$ and $D_{max} = 0.13\ m^2/d$ at
897 sensor spacing of $\Delta z = 0.1$ and $\Delta z = 0.2$ m. b) Same as a) but for the step change occurring at 8
898 different times (separated by 0.125 d or $\pi/4$) relative to the start of the harmonic temperature
899 signal used as boundary condition at $z = 0$ m (shown on right axis, with $D_{avg} = 0.075\ m^2/d$ and
900 sensor spacing $\Delta z = 0.2$ m.

901 Figure 4: Amplitude and phase response of common signal extraction methods (rows from top to
902 bottom: WFT, filtfilt, CWT and DHR) to the non-stationarity introduced by a step velocity
903 increase. Line color becomes lighter with increasing depth. Left column contains amplitudes,
904 right column contains phases. Note that the values obtained from filtfilt (c and d) are plotted
905 with dots whereas the lines are shown for visual improvement.

906 Figure 5: Vertical advective thermal velocities (left column: a, c, e, g) and thermal diffusivities
907 (right column: b, d, f, h) inverted using amplitudes and phases from peak picking applied to raw
908 data (red markers) as well as after applying 4 different signal processing methods (blue markers)
909 to the model temperature output. The different cases are in rows from top to bottom: 0 to -1 m/d

(a-b), 0 to 1 m/d (c-d), -1 m/d to 1 m/d (e-f), 1 m/d to -1 m/d (g-h). Refer to Figures 6 and 7 for different velocity steps.

Figure 6: Downward advective thermal velocities (left column: a, c, e, g) and thermal diffusivities (right column: b, d, f, h) inverted using amplitudes and phases from peak picking applied to raw data (red markers) as well as after applying 4 different signal processing methods (blue markers) to the model temperature output. The different cases are in rows from top to bottom: 0 to -0.01 m/d (a-b), 0 to -0.1 m/d (c-d), 0 m/d to -0.5 m/d (e-f), 0 m/d to -5 m/d (g-h).

Figure 7: Upward advective thermal velocities (left column: a, c, e) and thermal diffusivities (right column: b, d, f) inverted using amplitudes and phases from peak picking applied to raw data (red markers) as well as after applying 4 different signal processing methods (blue markers) to the model temperature output. The different cases are in rows from top to bottom: 0 to 0.1 m/d (a-b), 0 to 0.5 m/d (c-d), 0 m/d to 2 m/d (e-f).

Figure 8: Vertical advective thermal velocities (left column: a, c, e, g) and thermal diffusivities (right column: b, d, f, h) inverted using amplitudes and phases from peak picking applied to raw data (red markers) as well as after applying 4 different signal processing methods (blue markers) to the model temperature output. The different scenarios are a linear change of advective thermal velocity from 0 to -1 m/d over a total time period of (in rows from top to bottom): 0.5 days (a-b), 1 day (c-d), 2 days (e-f) and 4 days (g-h).

Figure 9: a) Temperature output obtained from the numerical model at different depths (0, 0.05, 0.2 and 0.4 m from the top of the sediment) using measured surface water temperature data as the top boundary (from Rau et al. [2010]). b) Advective thermal velocities and c) thermal diffusivities inverted after the data has been processed with 4 different amplitude and phase extraction methods.

Table captions

Table 1: Summary of maximum error and root mean square error (RMSE) calculated from modeled and inverted advective thermal velocities using unfiltered and filtered temperature data for the same magnitude velocity transients (0 to -1 m/d) but for different rates of velocity change. The values in this table represent a quantification of the results in Figure 8a, 8c, 8e, 8g and Figure 5a.

Table 2: Summary of maximum error and root mean square error (RMSE) calculated from modeled and inverted thermal diffusivities using unfiltered and filtered temperature data for the same magnitude velocity transients (0 to -1 m/d) but for different rates of velocity change. The values in this table represent a quantification of the results in Figure 8b, 8d, 8f, 8h and Figure 5b.

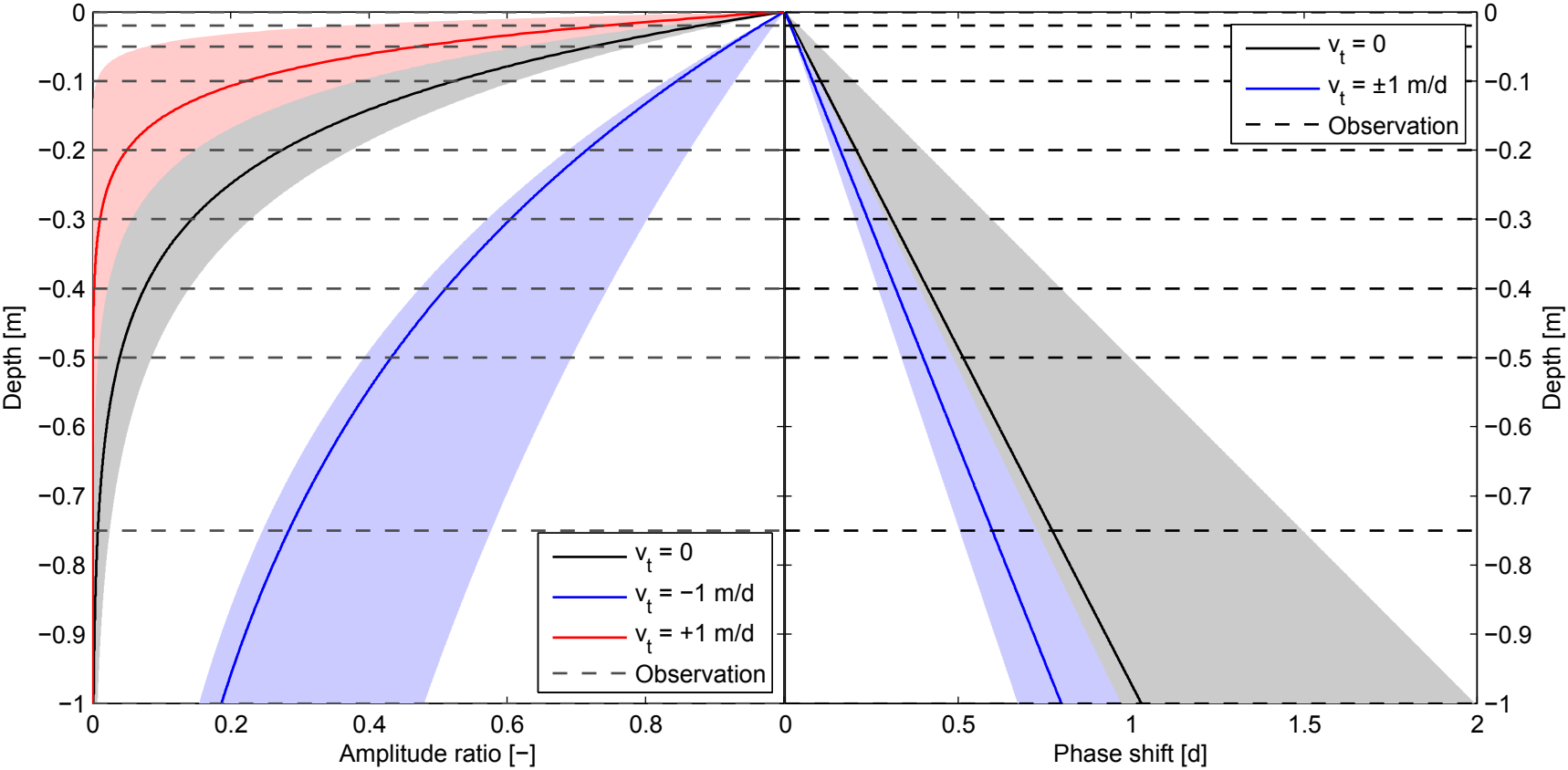
Depth [m]
0
−0.1
−0.2
−0.3
−0.4
−0.5
−0.6
−0.7
−0.8
−0.9
−1
0
0.2
0.4
0.6
0.8
Amplitude ratio [−]
v_t = 0
v_t = −1 m/d
v_t = +1 m/d
Observation
0
0.5
1
1.5
2
Phase shift [d]
v_t = 0
v_t = ±1 m/d
Observation
Depth [m]

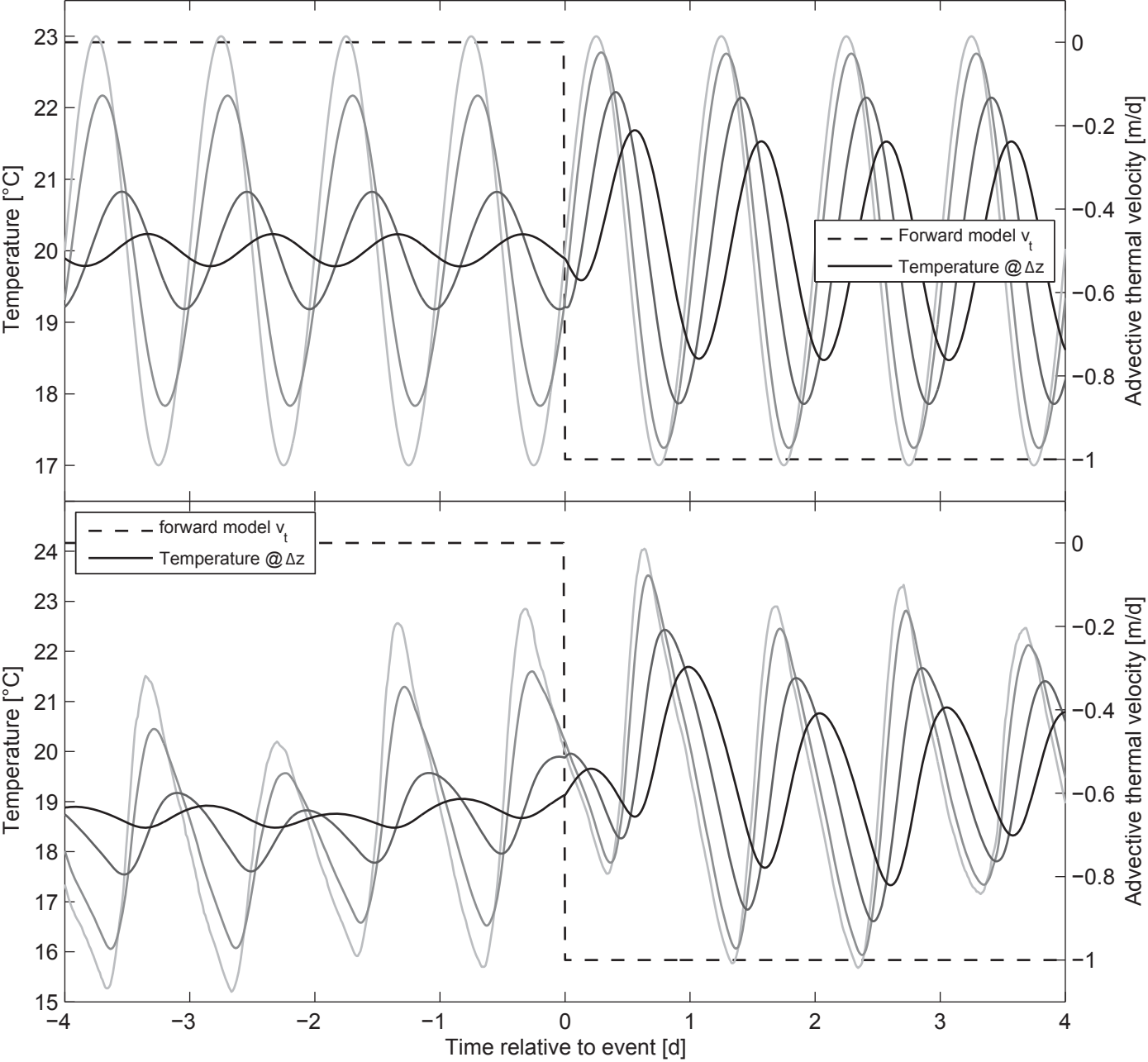
Temperature [°C]
Advective thermal velocity [m/d]
Forward model v_t
Temperature @ Δz
forward model v_t
Temperature @ Δz
Time relative to event [d]

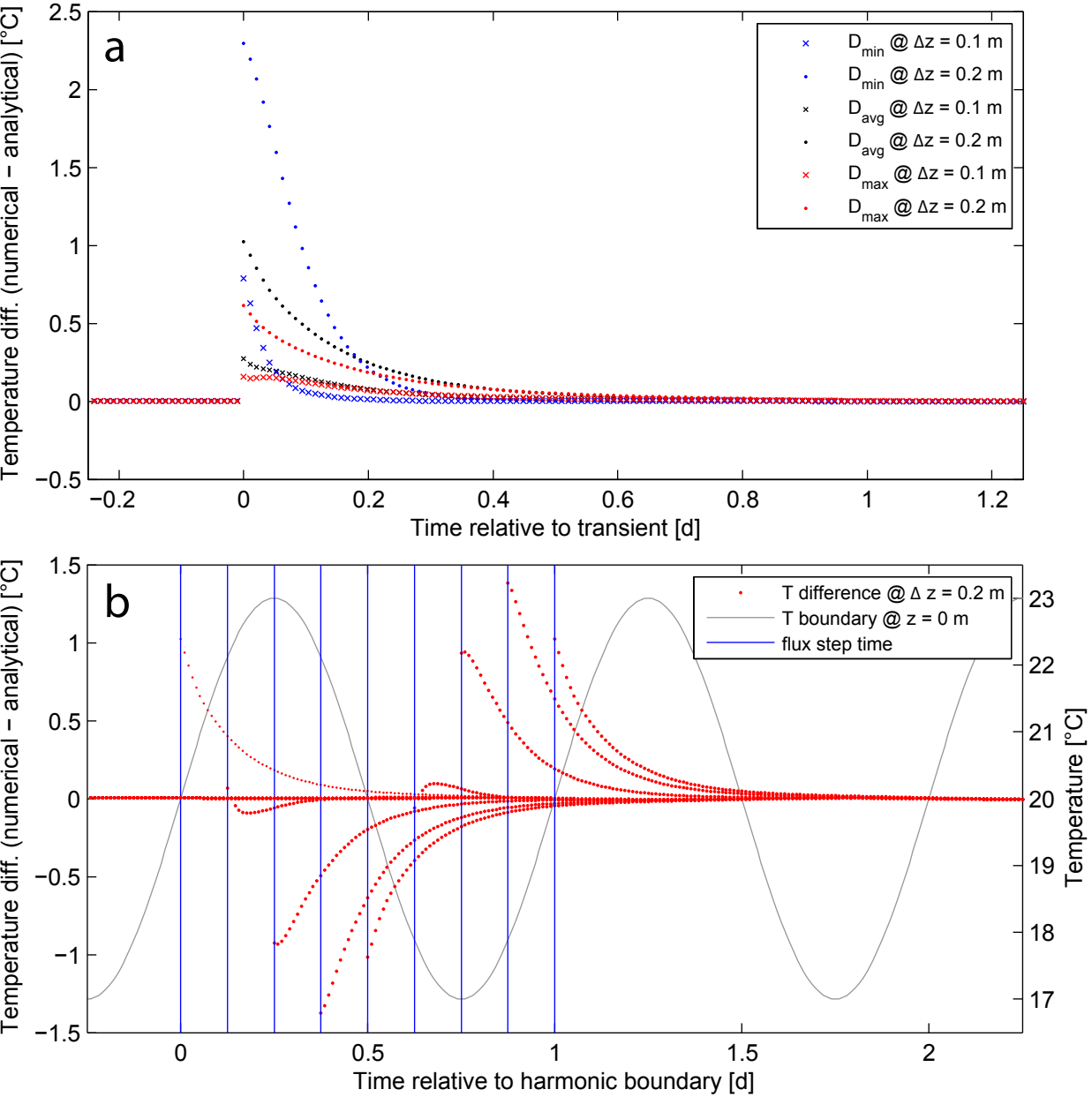
a
b
Temperature diff. (numerical − analytical) [°C]
Time relative to transient [d]
Time relative to harmonic boundary [d]
Temperature [°C]
D_min @ Δz = 0.1 m
D_min @ Δz = 0.2 m
D_avg @ Δz = 0.1 m
D_avg @ Δz = 0.2 m
D_max @ Δz = 0.1 m
D_max @ Δz = 0.2 m
T difference @ Δ z = 0.2 m
T boundary @ z = 0 m
flux step time

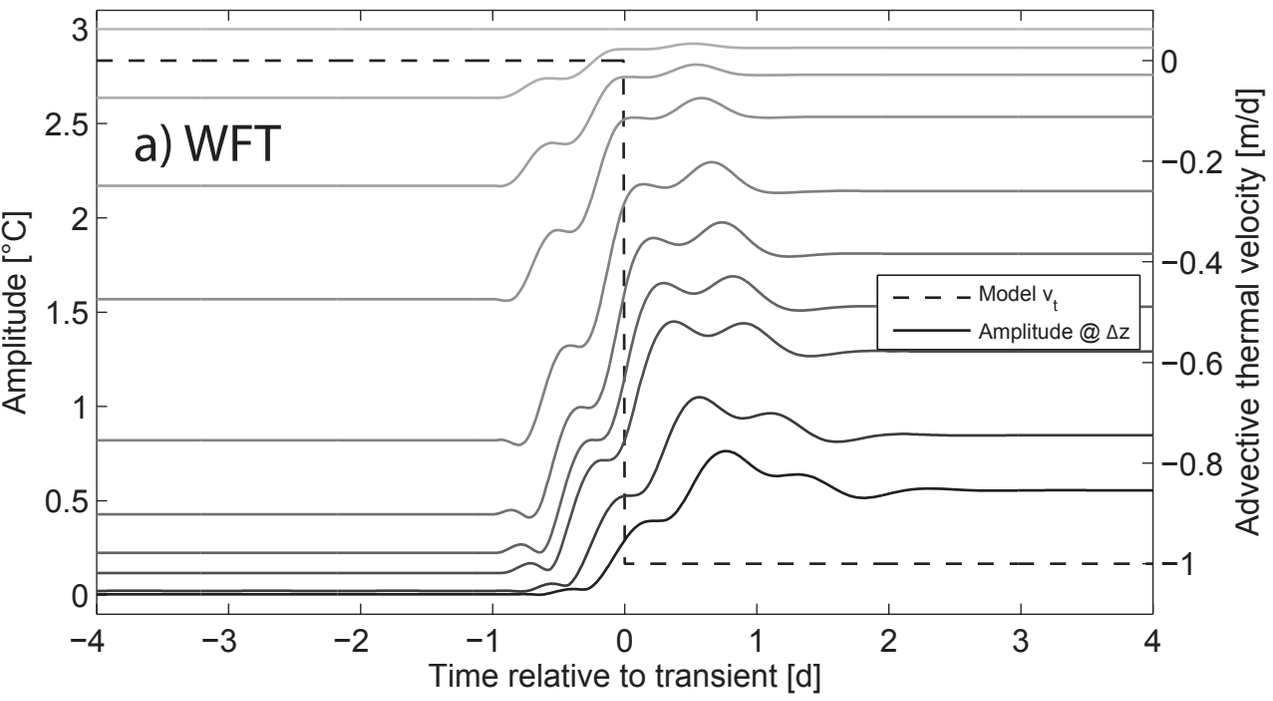
a) WFT
Amplitude [°C]
Advective thermal velocity [m/d]
Time relative to transient [d]
Model v_t
Amplitude @ Δz

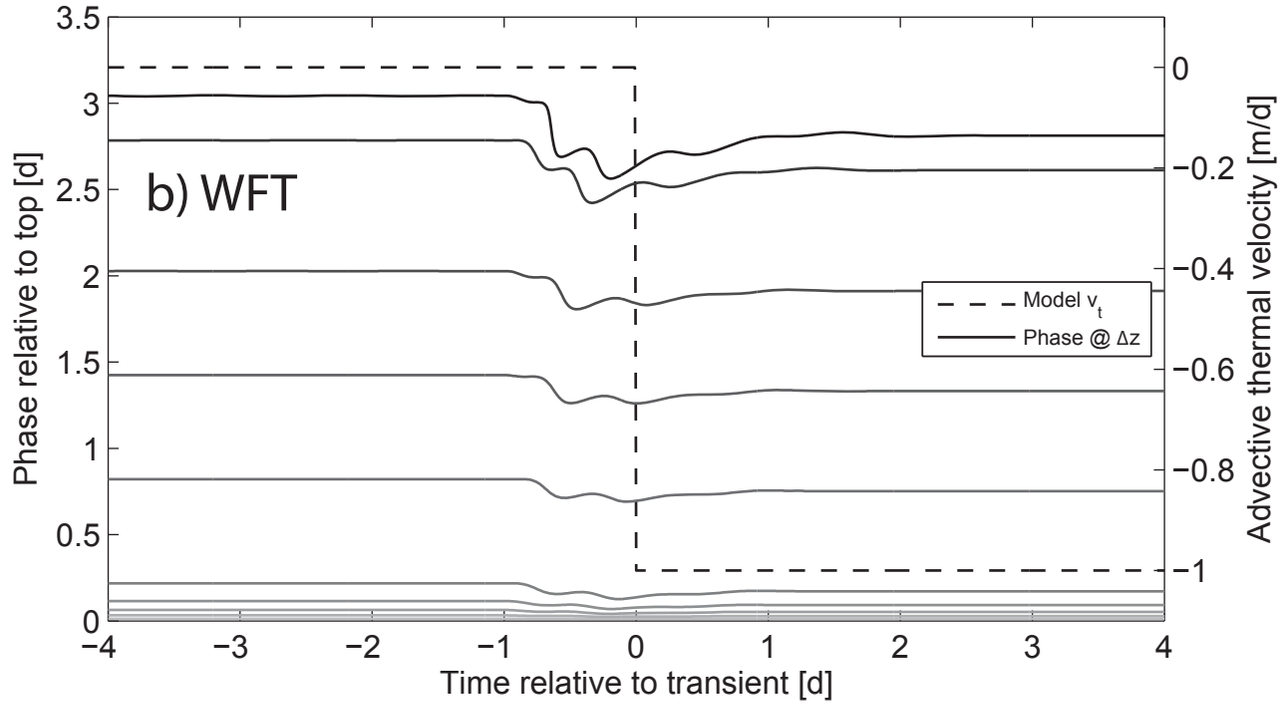
b) WFT
Phase relative to top [d]
Advective thermal velocity [m/d]
Time relative to transient [d]
Model v_t
Phase @ Δz

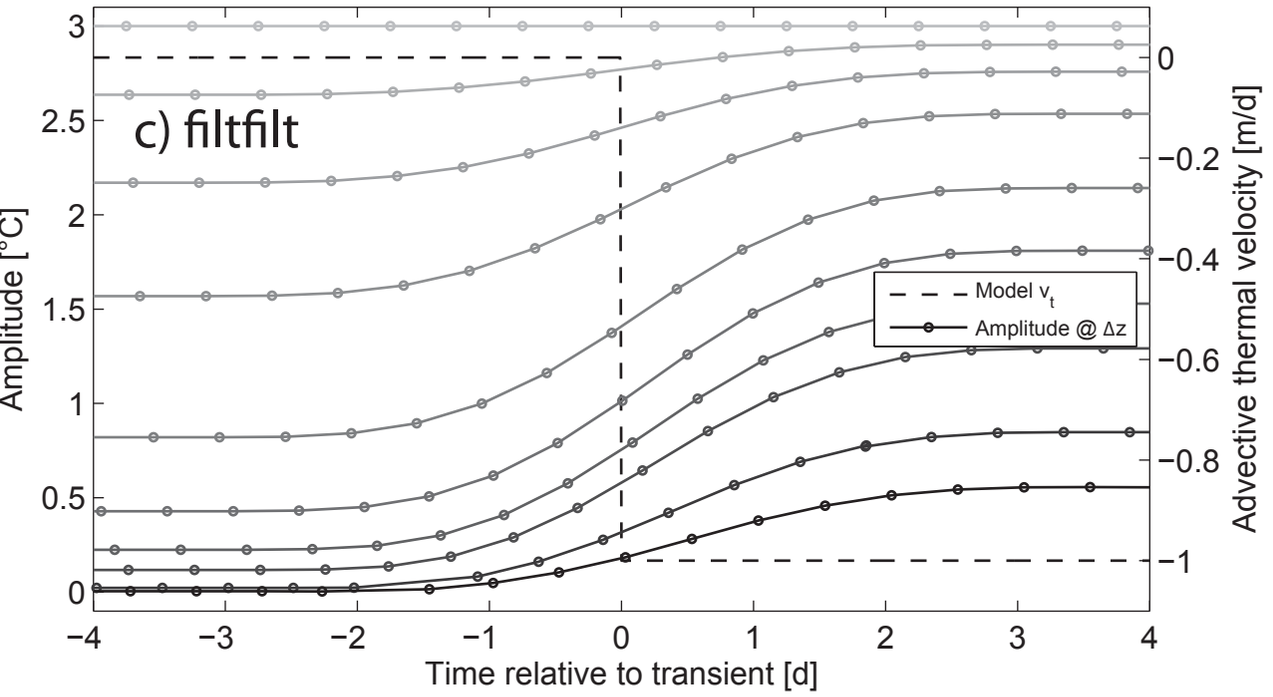
c) filtfilt
Amplitude [°C]
Advective thermal velocity [m/d]
Time relative to transient [d]
Model v_t
Amplitude @ Δz

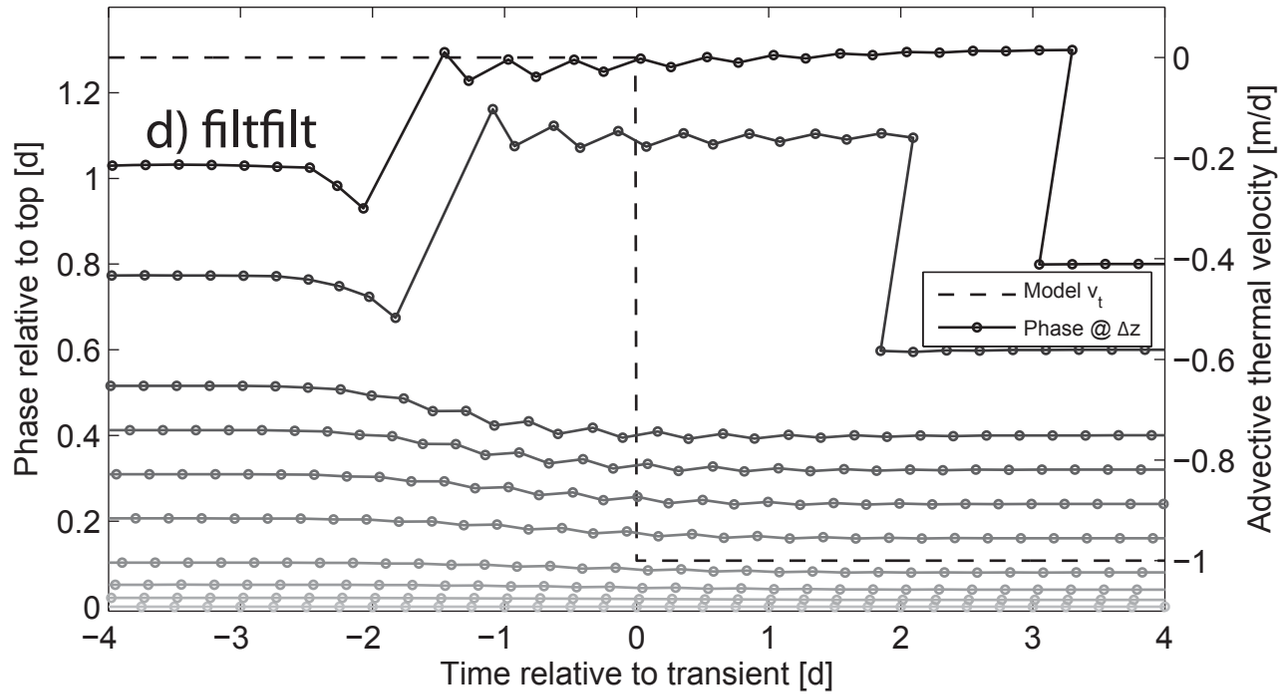
d) filtfilt
Phase relative to top [d]
Advective thermal velocity [m/d]
Time relative to transient [d]
Model v_t
Phase @ Δz

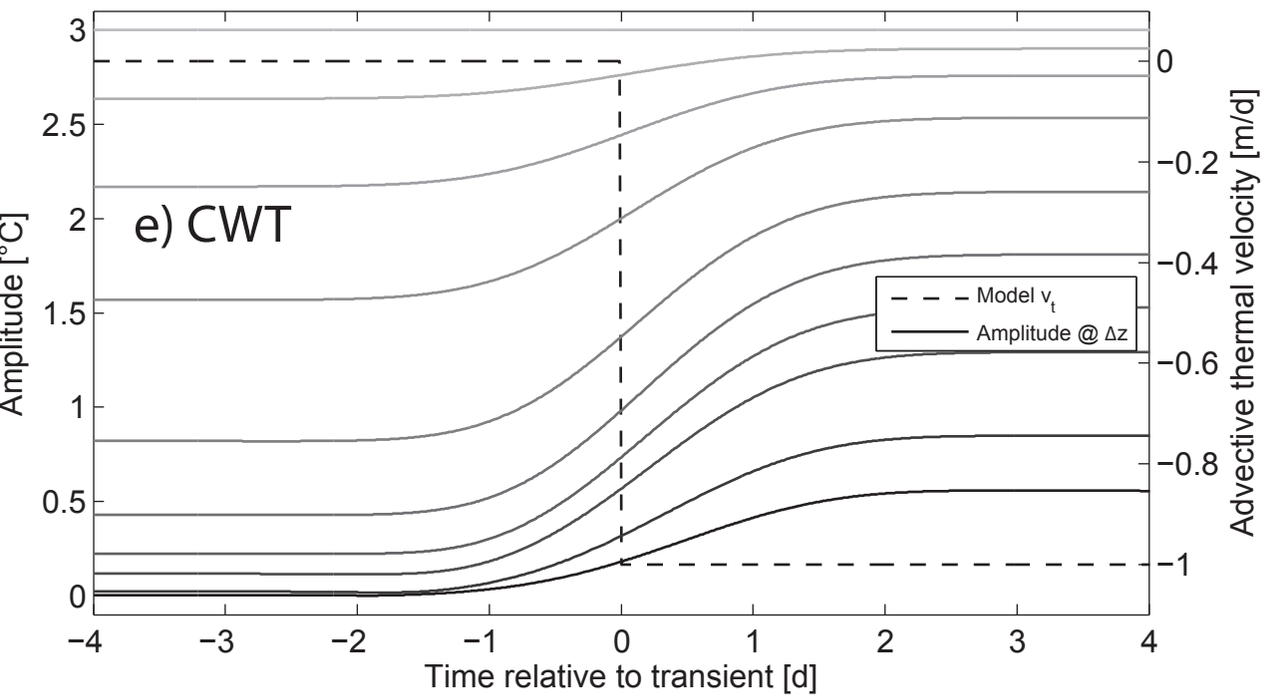
e) CWT
Amplitude [°C]
Advective thermal velocity [m/d]
Time relative to transient [d]
Model v_t
Amplitude @ Δz

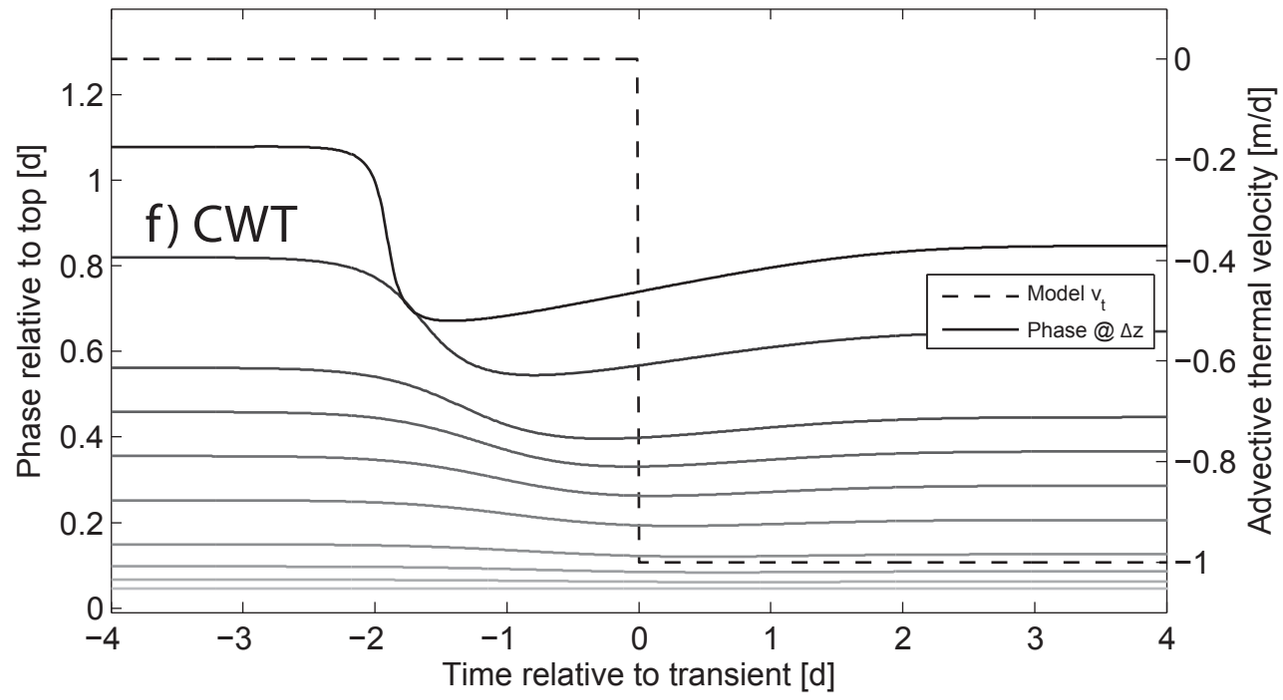
f) CWT
Phase relative to top [d]
Advective thermal velocity [m/d]
Time relative to transient [d]
Model v_t
Phase @ Δz

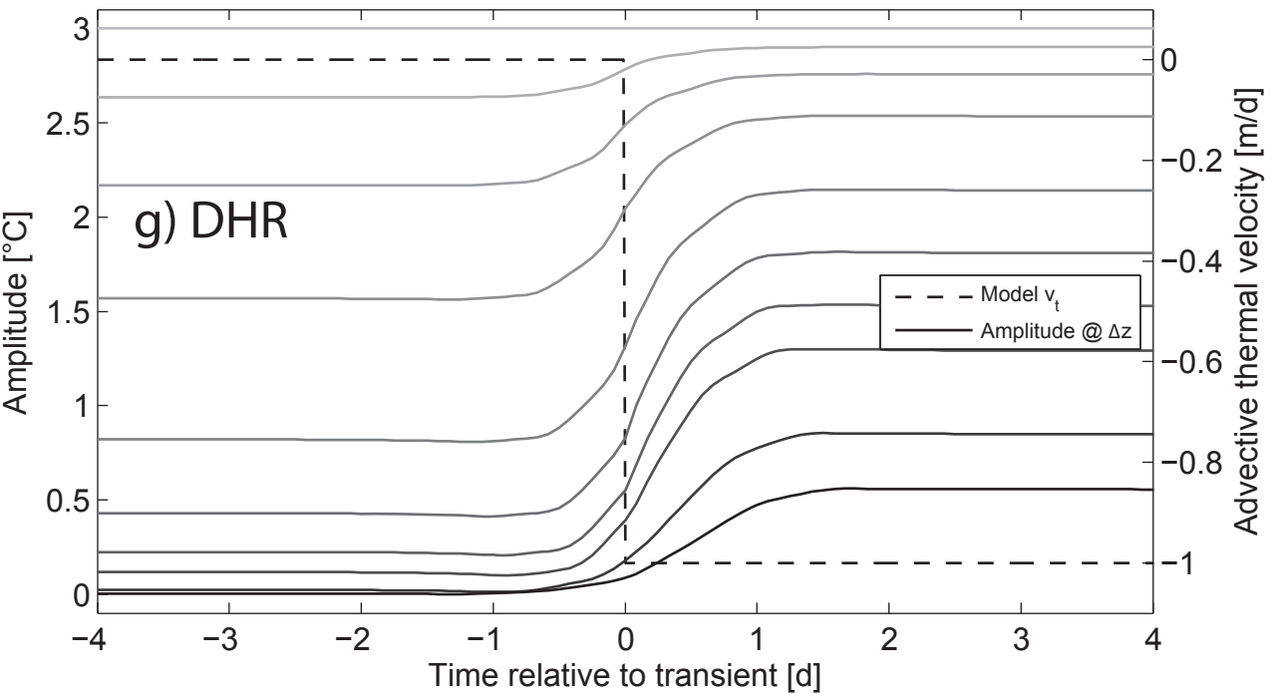
g) DHR
Amplitude [°C]
Advective thermal velocity [m/d]
Time relative to transient [d]
Model v_t
Amplitude @ Δz

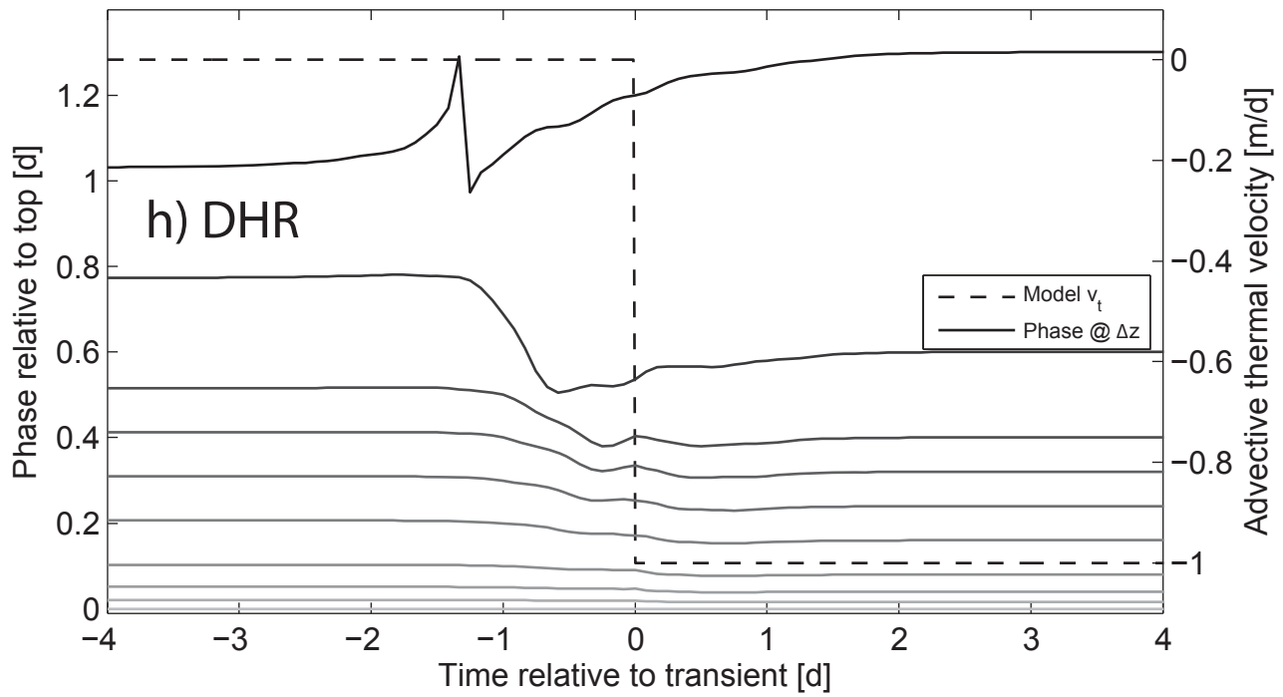
h) DHR
Phase relative to top [d]
Advective thermal velocity [m/d]
Time relative to transient [d]
Model v_t
Phase @ Δz

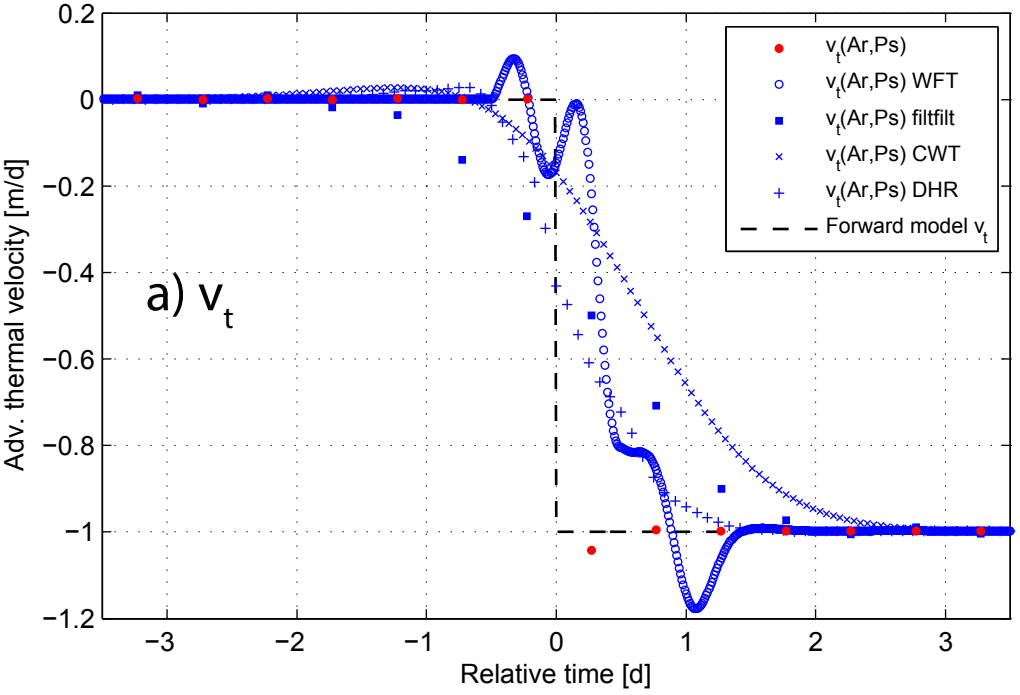
a) v_t
Adv. thermal velocity [m/d]
Relative time [d]
v_t(Ar,Ps)
v_t(Ar,Ps) WFT
v_t(Ar,Ps) filtfilt
v_t(Ar,Ps) CWT
v_t(Ar,Ps) DHR
Forward model v_t

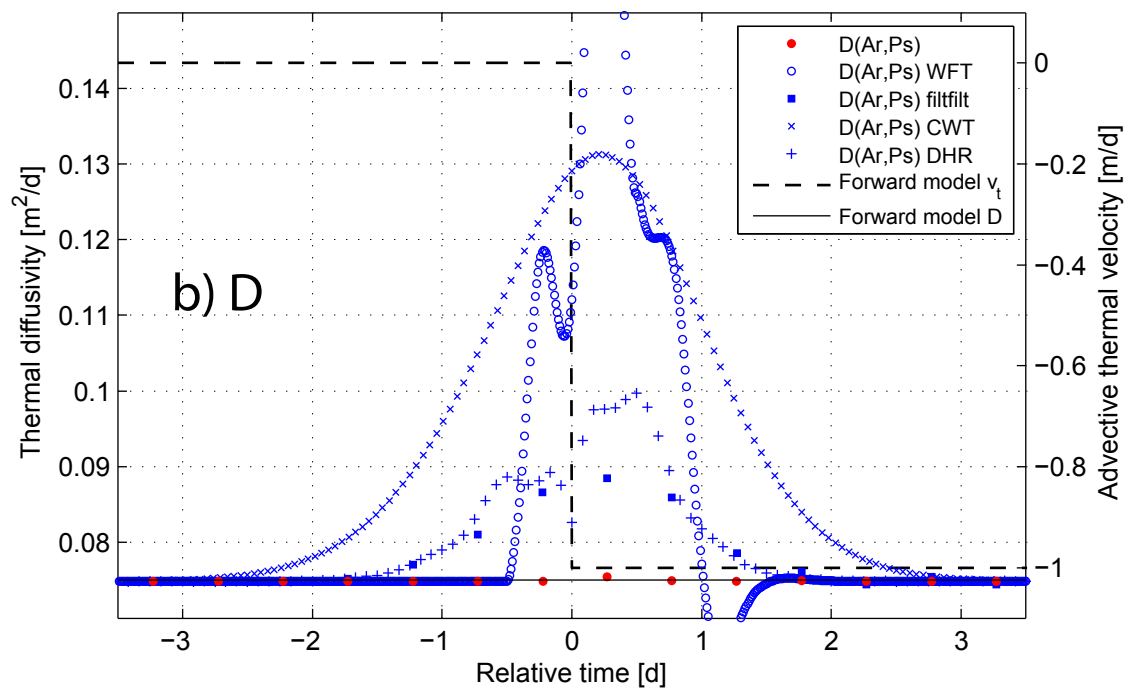
b) D
Thermal diffusivity [m²/d]
Advective thermal velocity [m/d]
Relative time [d]
D(Ar,Ps)
D(Ar,Ps) WFT
D(Ar,Ps) filtfilt
D(Ar,Ps) CWT
D(Ar,Ps) DHR
Forward model v_t
Forward model D

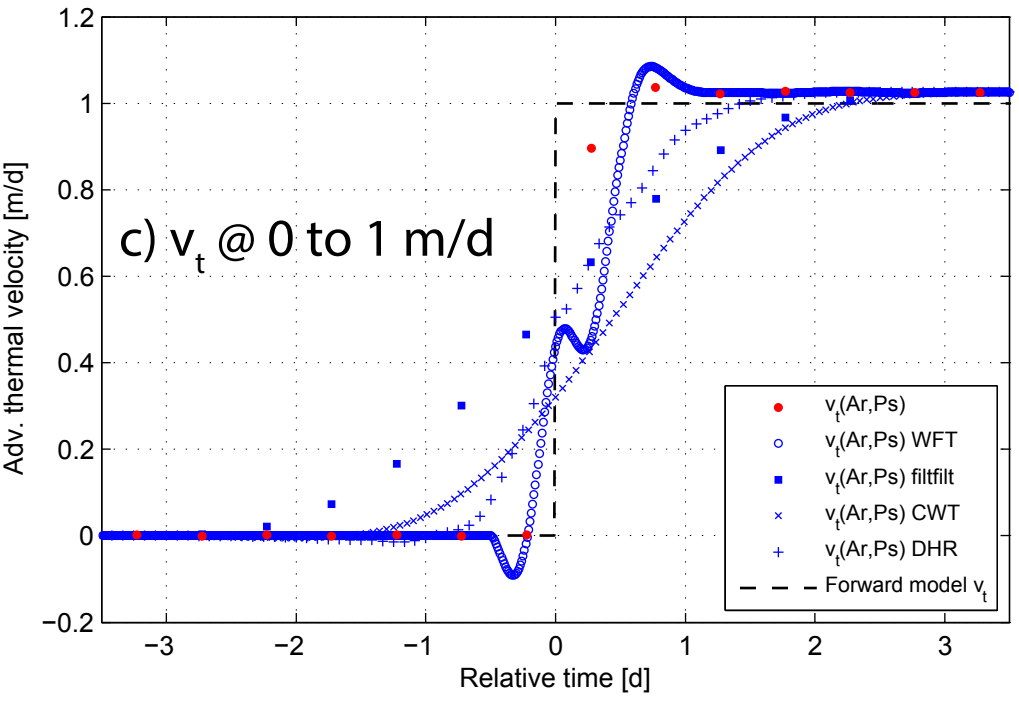
c) v_t @ 0 to 1 m/d
Adv. thermal velocity [m/d]
Relative time [d]
v_t(Ar,Ps)
v_t(Ar,Ps) WFT
v_t(Ar,Ps) filtfilt
v_t(Ar,Ps) CWT
v_t(Ar,Ps) DHR
Forward model v_t

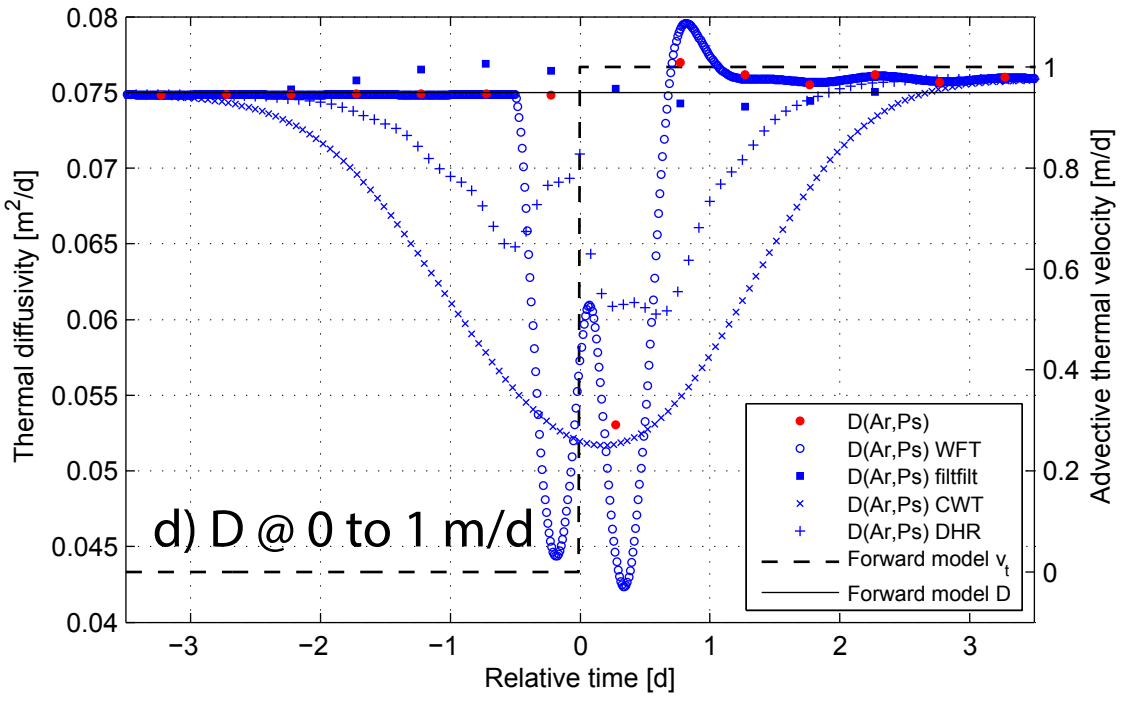
d) D @ 0 to 1 m/d
Thermal diffusivity [m²/d]
Advective thermal velocity [m/d]
Relative time [d]
D(Ar,Ps)
D(Ar,Ps) WFT
D(Ar,Ps) filtfilt
D(Ar,Ps) CWT
D(Ar,Ps) DHR
Forward model v_t
Forward model D

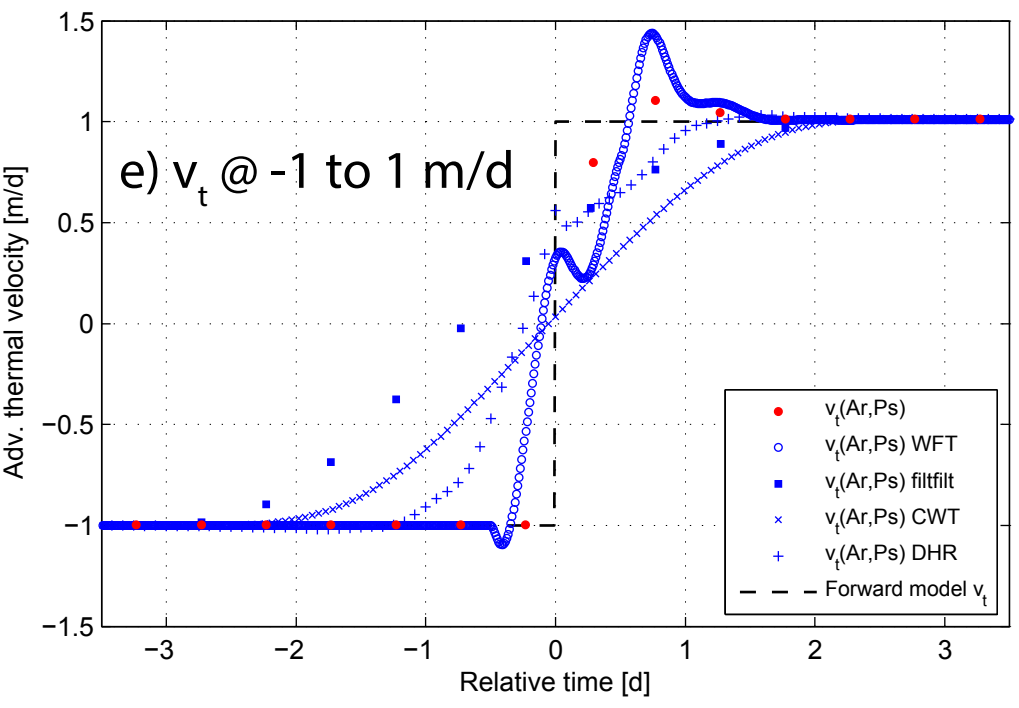
e) v_t @ -1 to 1 m/d
Adv. thermal velocity [m/d]
Relative time [d]
v_t(Ar,Ps)
v_t(Ar,Ps) WFT
v_t(Ar,Ps) filtfilt
v_t(Ar,Ps) CWT
v_t(Ar,Ps) DHR
Forward model v_t

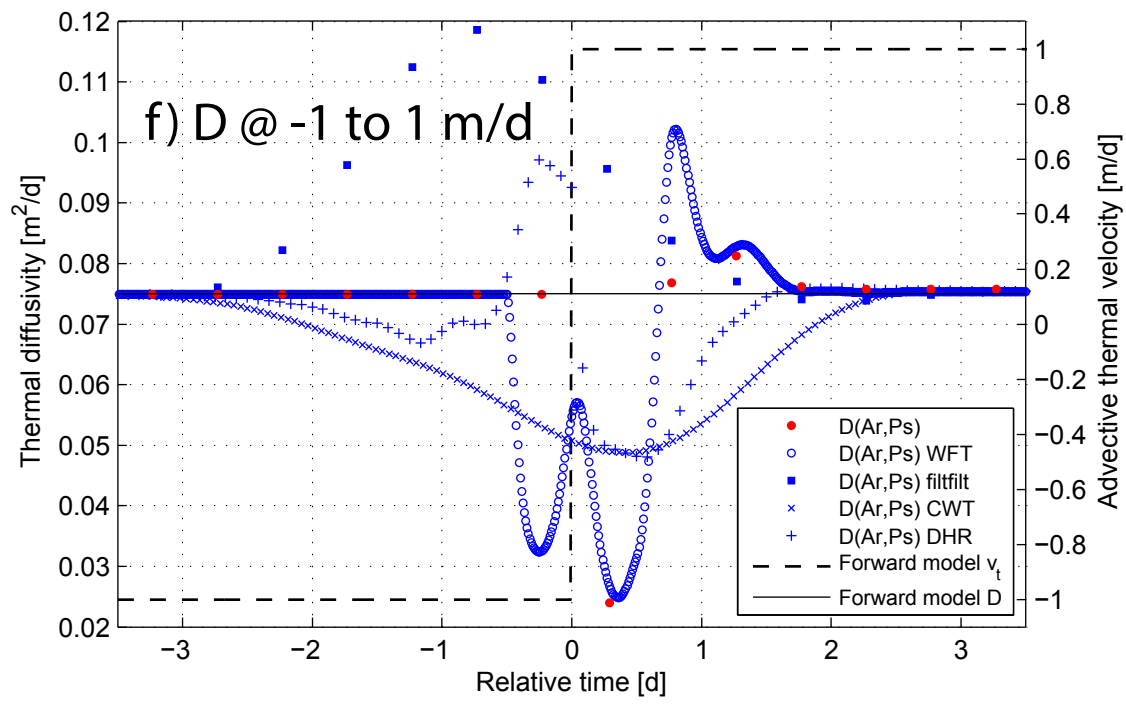
f) D @ -1 to 1 m/d
Thermal diffusivity [m²/d]
Advective thermal velocity [m/d]
Relative time [d]
D(Ar,Ps)
D(Ar,Ps) WFT
D(Ar,Ps) filtfilt
D(Ar,Ps) CWT
D(Ar,Ps) DHR
Forward model v_t
Forward model D

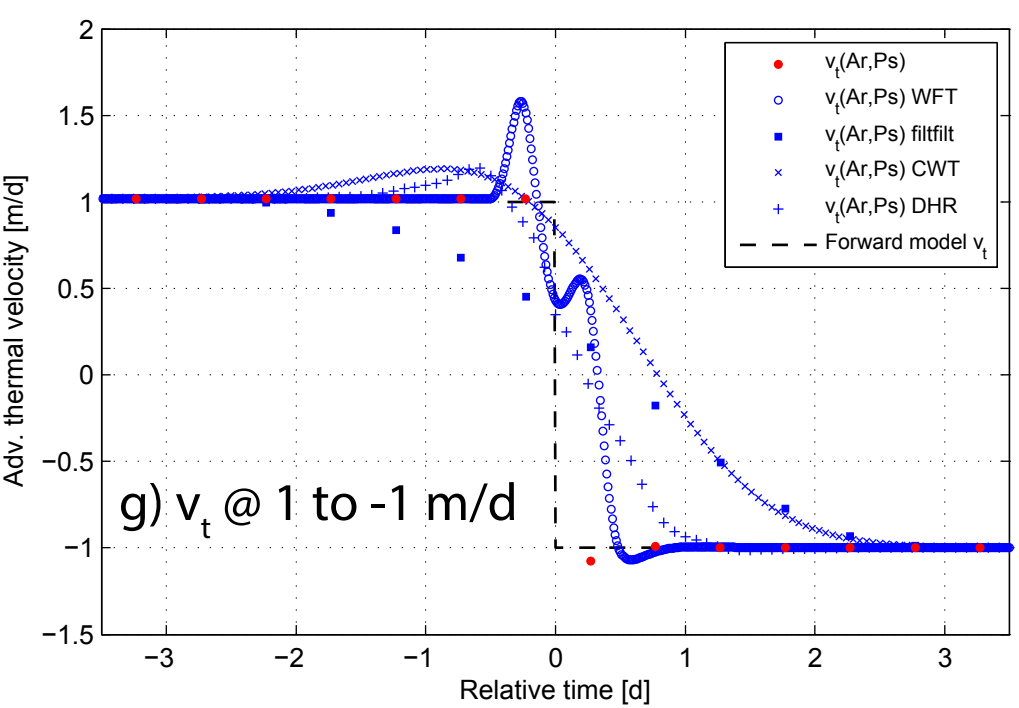
g) v_t @ 1 to -1 m/d
Adv. thermal velocity [m/d]
Relative time [d]
v_t(Ar,Ps)
v_t(Ar,Ps) WFT
v_t(Ar,Ps) filtfilt
v_t(Ar,Ps) CWT
v_t(Ar,Ps) DHR
Forward model v_t

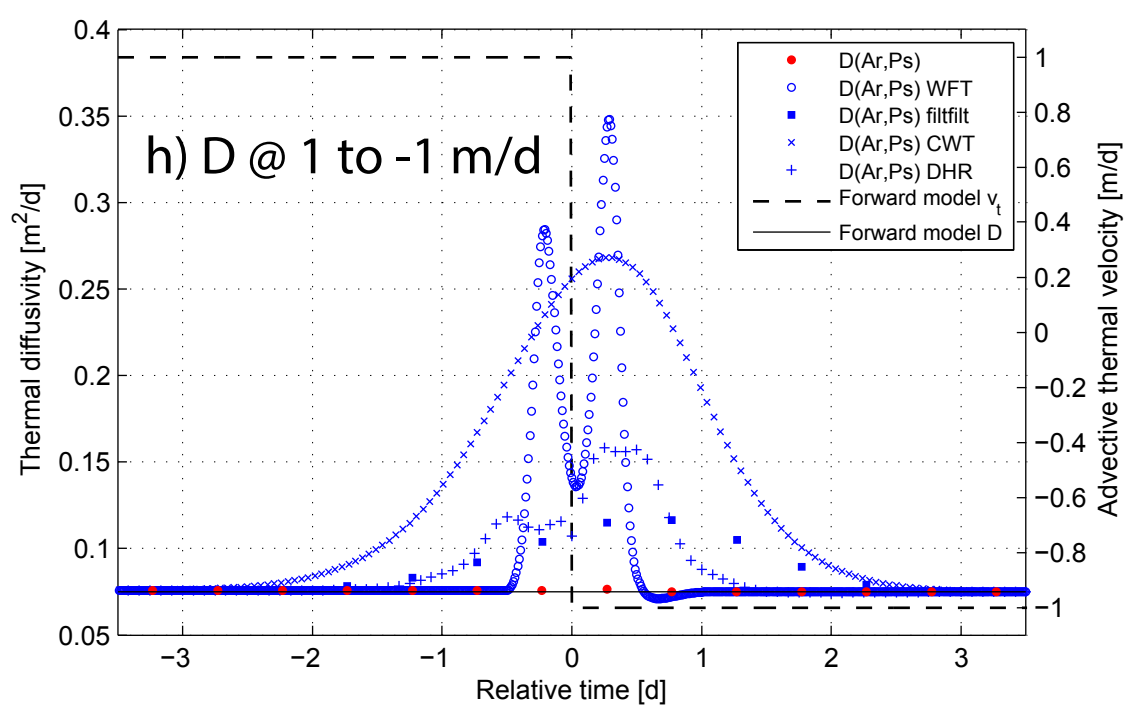
h) D @ 1 to -1 m/d
Thermal diffusivity [m²/d]
Advective thermal velocity [m/d]
Relative time [d]
D(Ar,Ps)
D(Ar,Ps) WFT
D(Ar,Ps) filtfilt
D(Ar,Ps) CWT
D(Ar,Ps) DHR
Forward model v_t
Forward model D

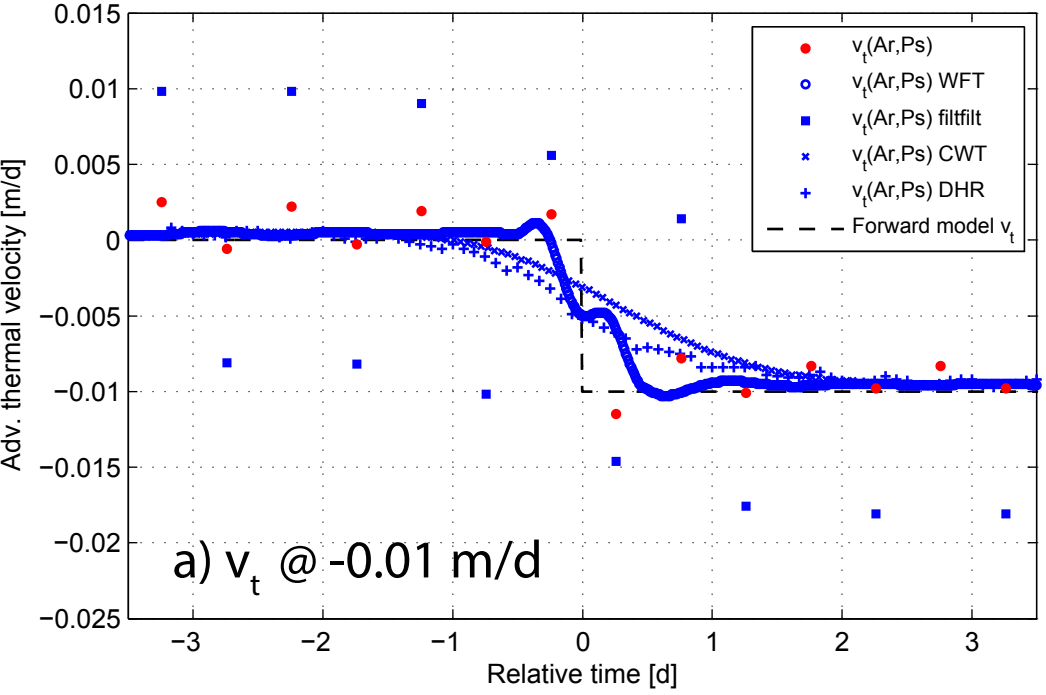
a) v_t @ -0.01 m/d
Adv. thermal velocity [m/d]
Relative time [d]
v_t(Ar,Ps)
v_t(Ar,Ps) WFT
v_t(Ar,Ps) filtfilt
v_t(Ar,Ps) CWT
v_t(Ar,Ps) DHR
Forward model v_t

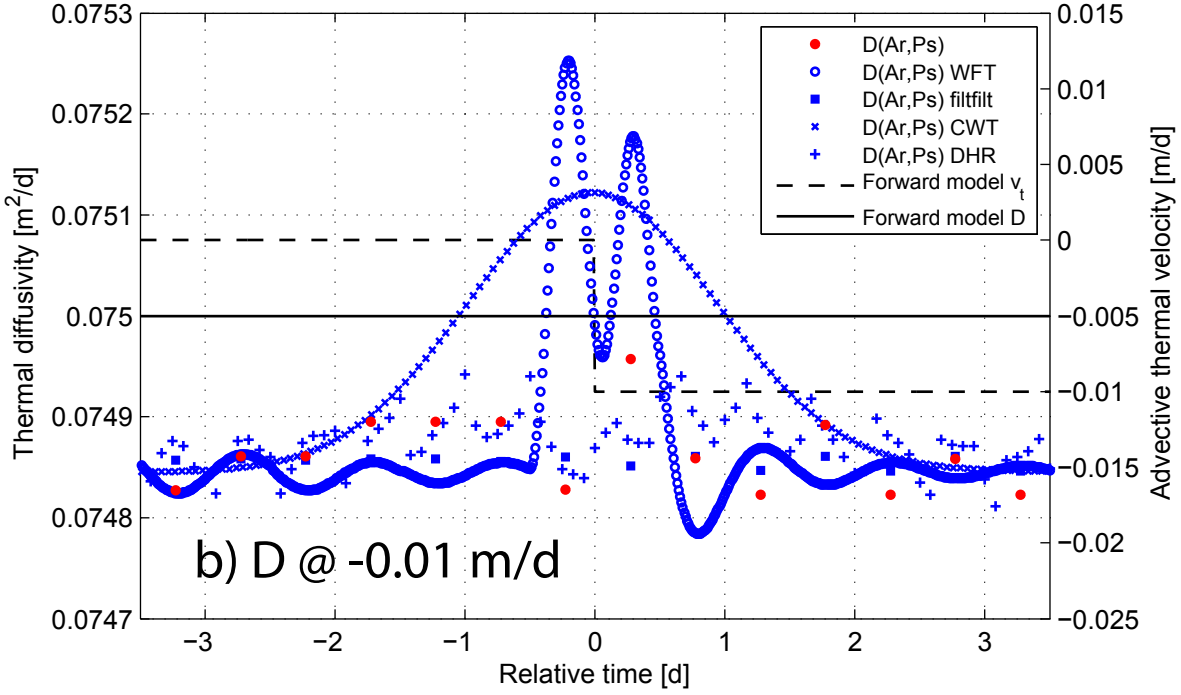
b) D @ -0.01 m/d
Thermal diffusivity [m²/d]
Advective thermal velocity [m/d]
Relative time [d]
D(Ar,Ps)
D(Ar,Ps) WFT
D(Ar,Ps) filtfilt
D(Ar,Ps) CWT
D(Ar,Ps) DHR
Forward model v_t
Forward model D

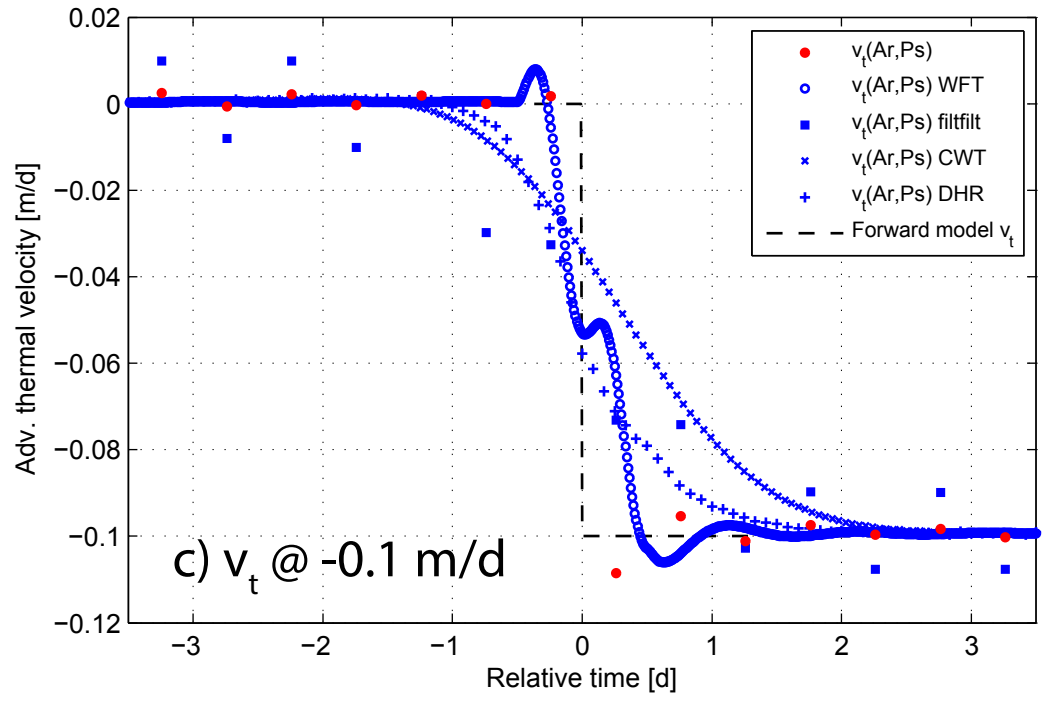
c) v_t @ -0.1 m/d
Adv. thermal velocity [m/d]
Relative time [d]
v_t(Ar,Ps)
v_t(Ar,Ps) WFT
v_t(Ar,Ps) filtfilt
v_t(Ar,Ps) CWT
v_t(Ar,Ps) DHR
Forward model v_t

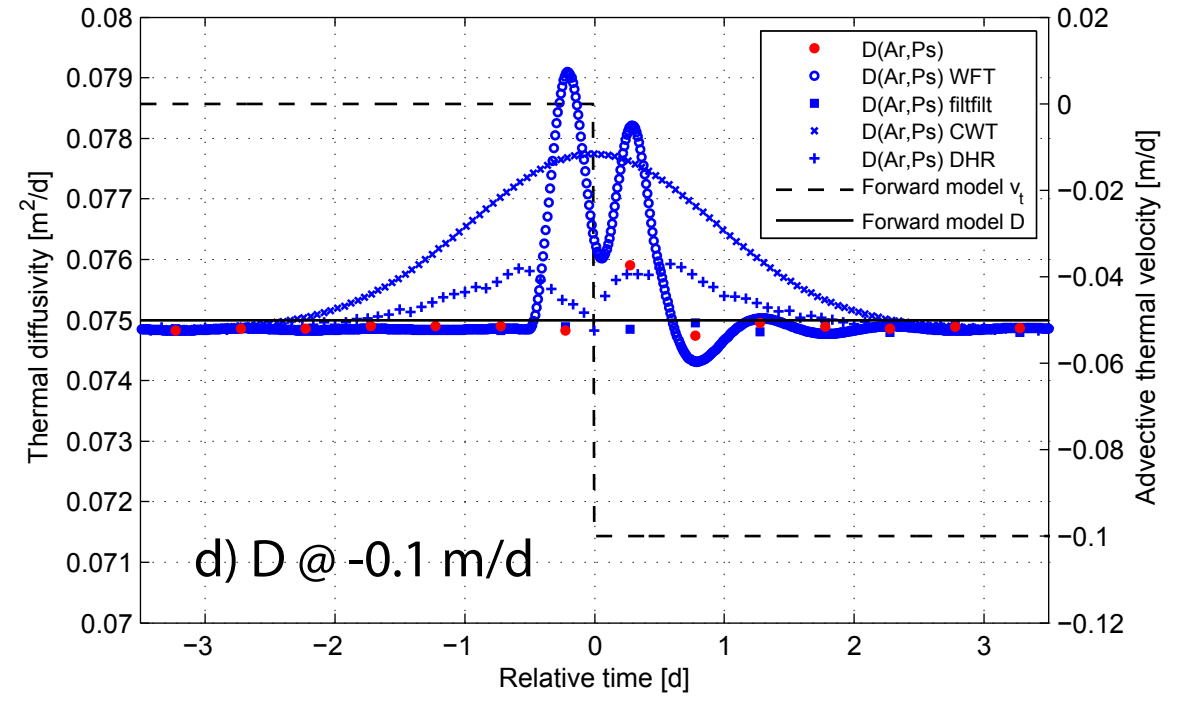
d) D @ -0.1 m/d
Thermal diffusivity [m²/d]
Advective thermal velocity [m/d]
Relative time [d]
D(Ar,Ps)
D(Ar,Ps) WFT
D(Ar,Ps) filtfilt
D(Ar,Ps) CWT
D(Ar,Ps) DHR
Forward model v_t
Forward model D

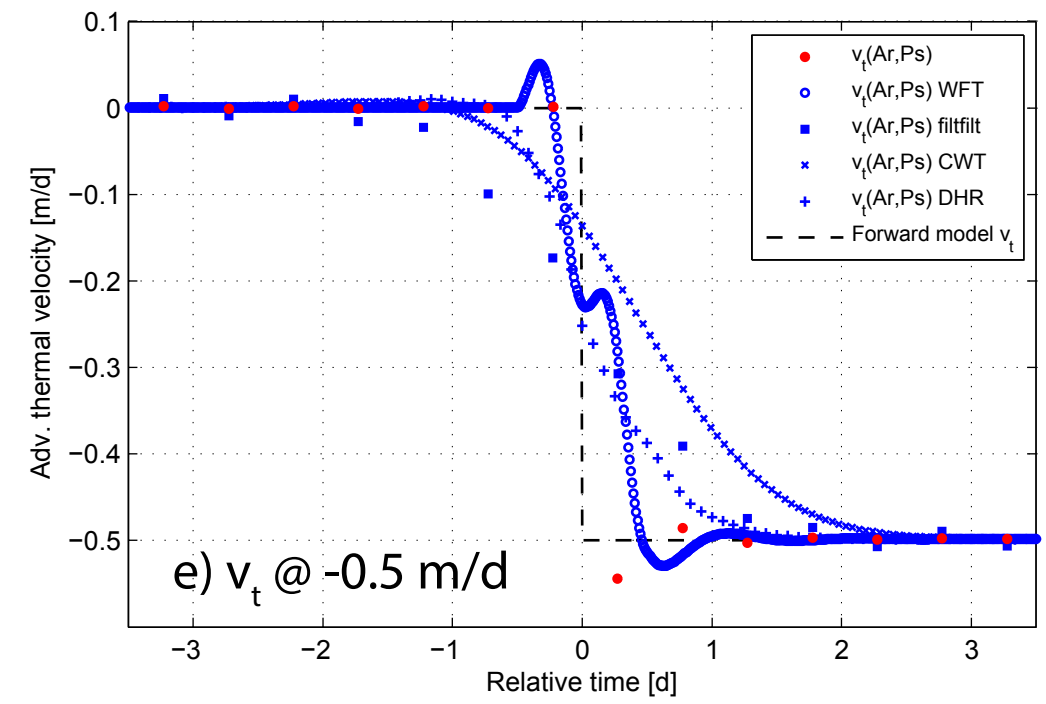
e) v_t @ -0.5 m/d
Adv. thermal velocity [m/d]
Relative time [d]
v_t(Ar,Ps)
v_t(Ar,Ps) WFT
v_t(Ar,Ps) filtfilt
v_t(Ar,Ps) CWT
v_t(Ar,Ps) DHR
Forward model v_t

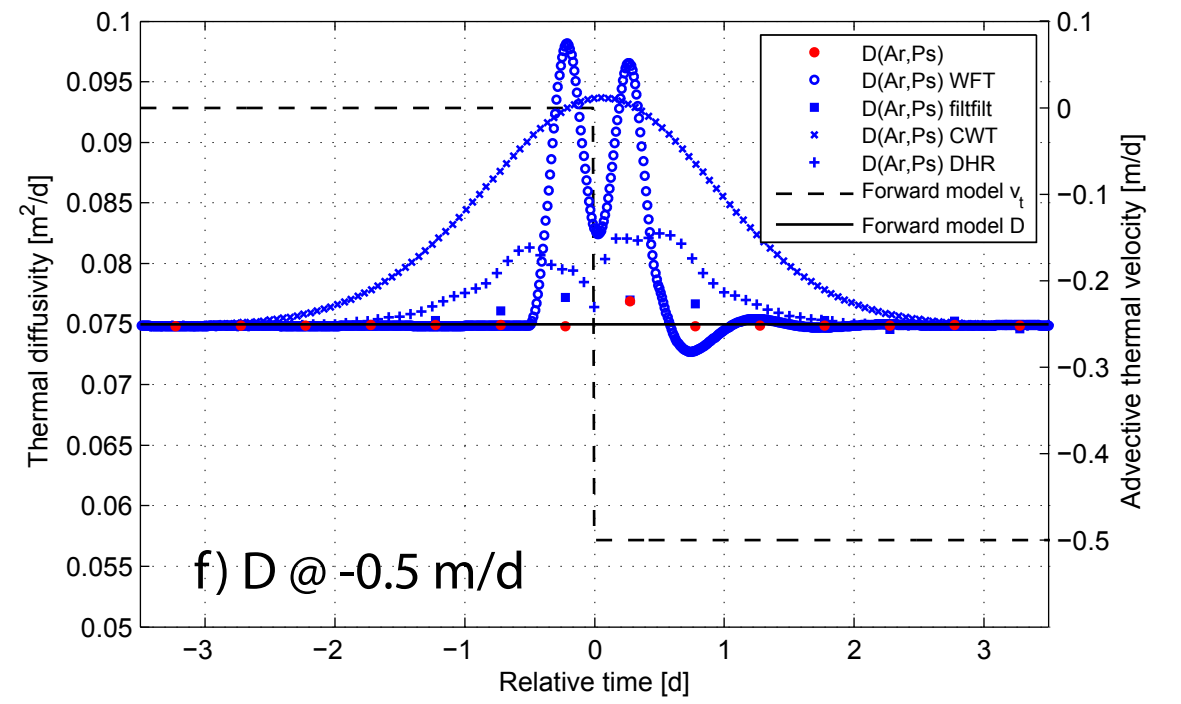
f) D @ -0.5 m/d
Thermal diffusivity [m²/d]
Advective thermal velocity [m/d]
Relative time [d]
D(Ar,Ps)
D(Ar,Ps) WFT
D(Ar,Ps) filtfilt
D(Ar,Ps) CWT
D(Ar,Ps) DHR
Forward model v_t
Forward model D

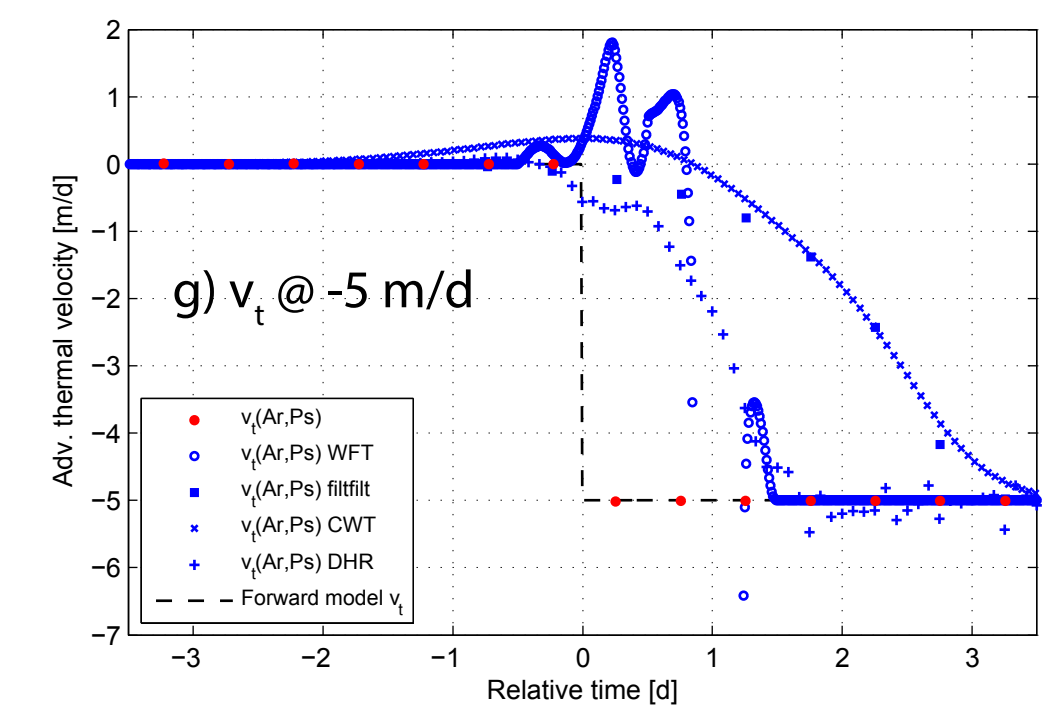
g) v_t @ -5 m/d
Adv. thermal velocity [m/d]
Relative time [d]
v_t(Ar,Ps)
v_t(Ar,Ps) WFT
v_t(Ar,Ps) filtfilt
v_t(Ar,Ps) CWT
v_t(Ar,Ps) DHR
Forward model v_t

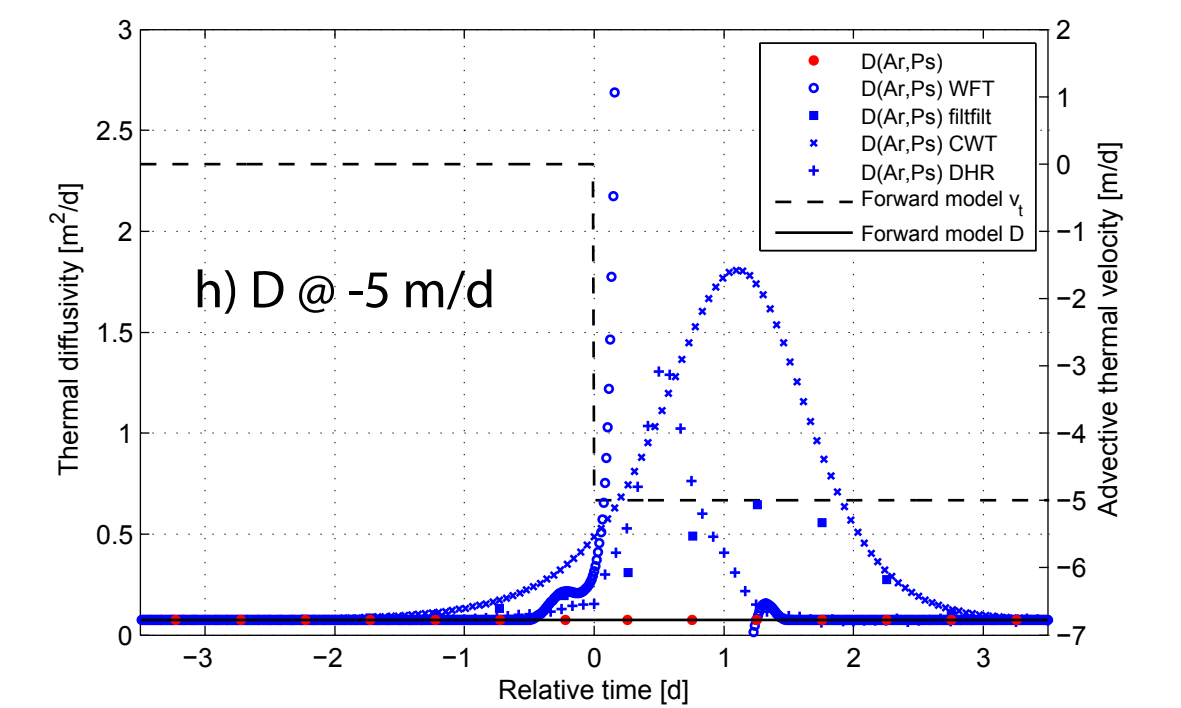
h) D @ -5 m/d
Thermal diffusivity [m²/d]
Advective thermal velocity [m/d]
Relative time [d]
D(Ar,Ps)
D(Ar,Ps) WFT
D(Ar,Ps) filtfilt
D(Ar,Ps) CWT
D(Ar,Ps) DHR
Forward model v_t
Forward model D

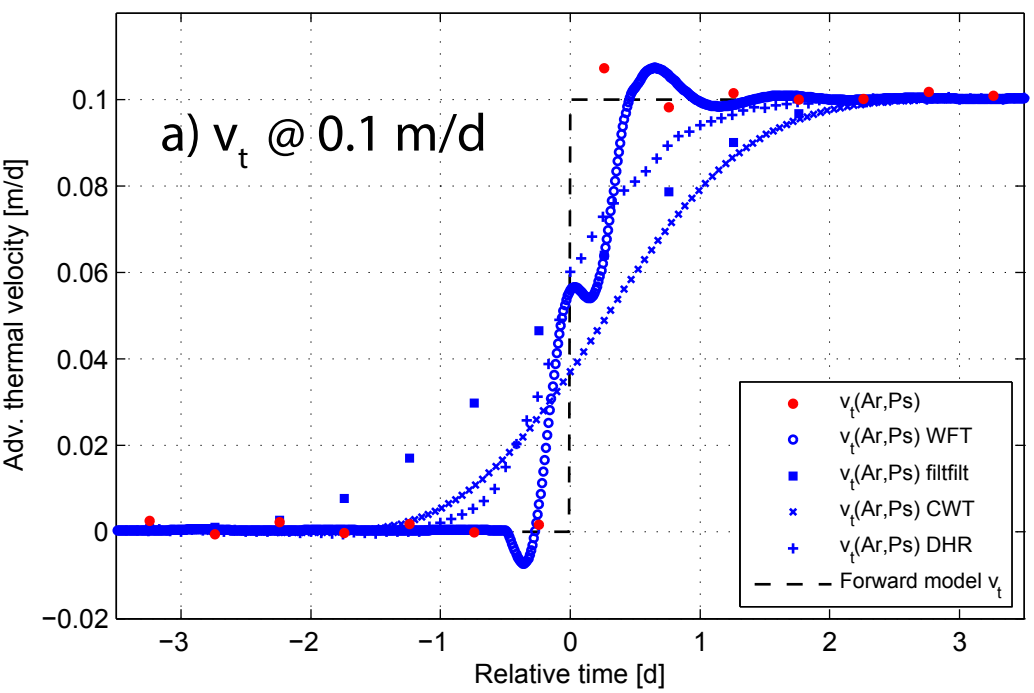
a) v_t @ 0.1 m/d
Adv. thermal velocity [m/d]
Relative time [d]
v_t(Ar,Ps)
v_t(Ar,Ps) WFT
v_t(Ar,Ps) filtfilt
v_t(Ar,Ps) CWT
v_t(Ar,Ps) DHR
Forward model v_t

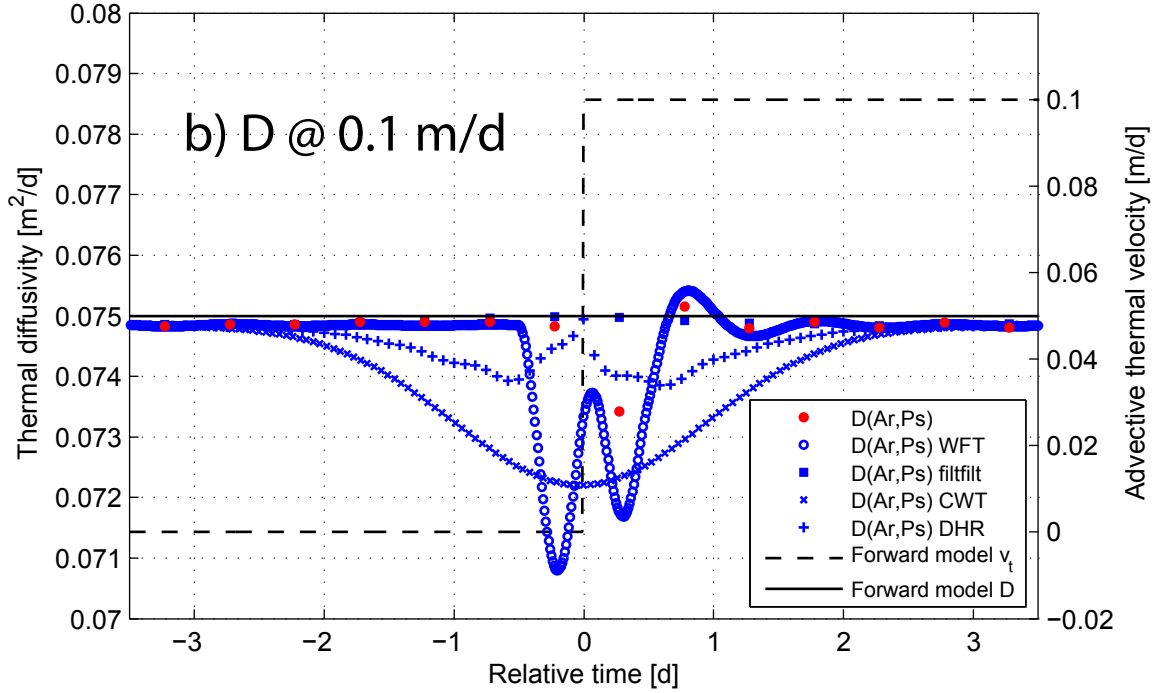
b) D @ 0.1 m/d
Thermal diffusivity [m²/d]
Advective thermal velocity [m/d]
Relative time [d]
D(Ar,Ps)
D(Ar,Ps) WFT
D(Ar,Ps) filtfilt
D(Ar,Ps) CWT
D(Ar,Ps) DHR
Forward model v_t
Forward model D

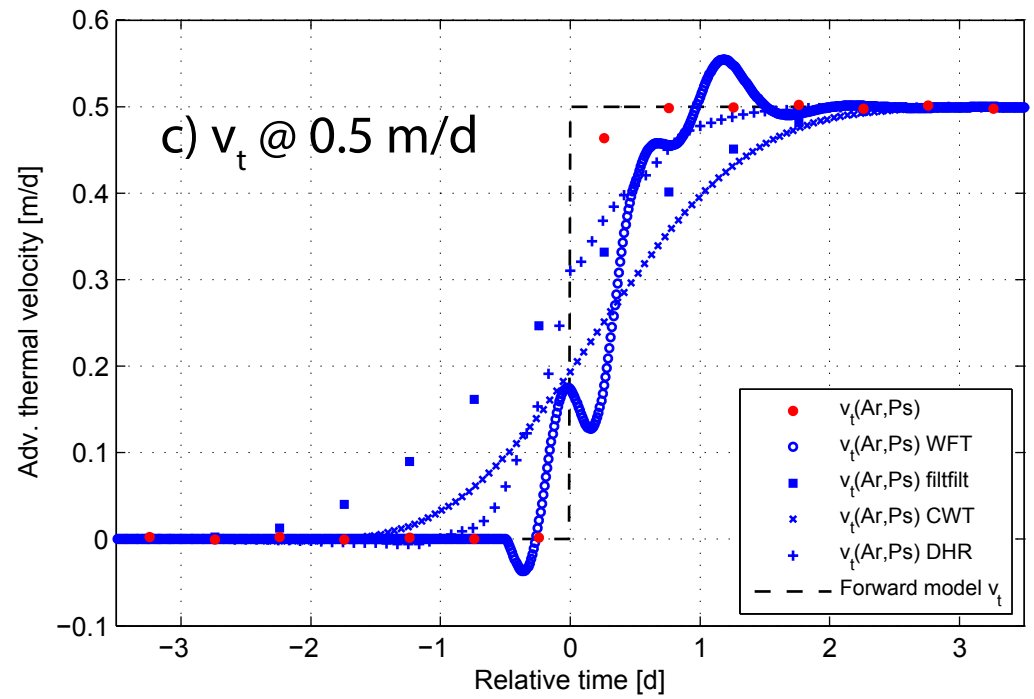
c) v_t @ 0.5 m/d
Adv. thermal velocity [m/d]
Relative time [d]
v_t(Ar,Ps)
v_t(Ar,Ps) WFT
v_t(Ar,Ps) filtfilt
v_t(Ar,Ps) CWT
v_t(Ar,Ps) DHR
Forward model v_t

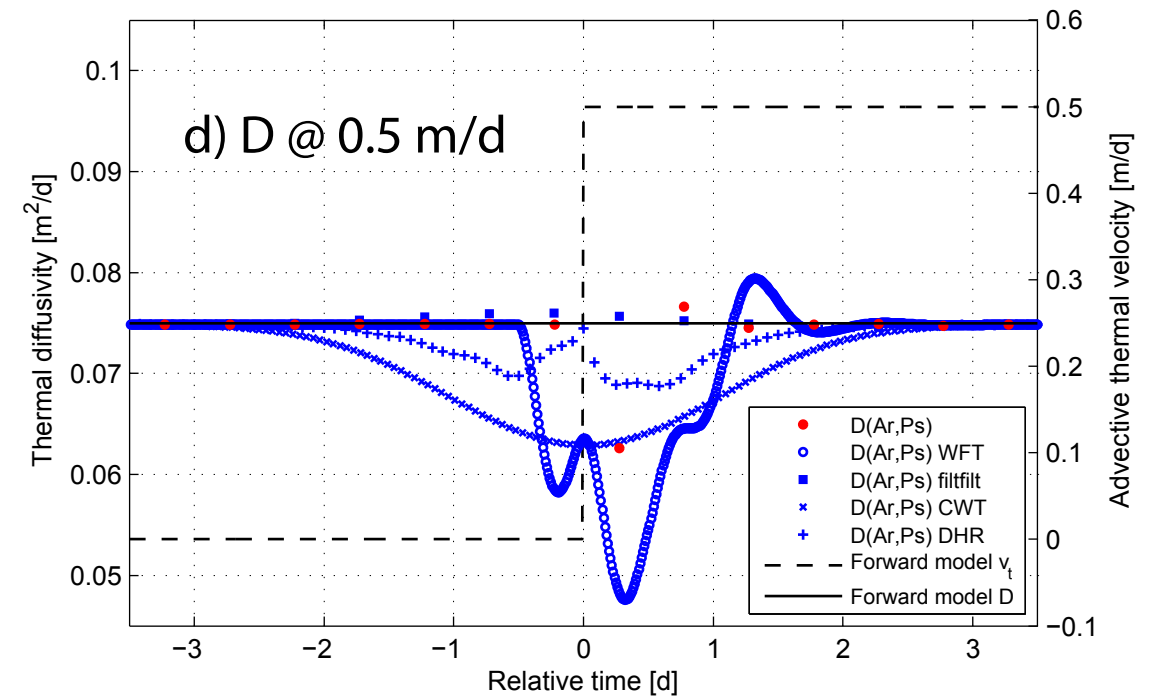
d) D @ 0.5 m/d
Thermal diffusivity [m²/d]
Advective thermal velocity [m/d]
Relative time [d]
D(Ar,Ps)
D(Ar,Ps) WFT
D(Ar,Ps) filtfilt
D(Ar,Ps) CWT
D(Ar,Ps) DHR
Forward model v_t
Forward model D

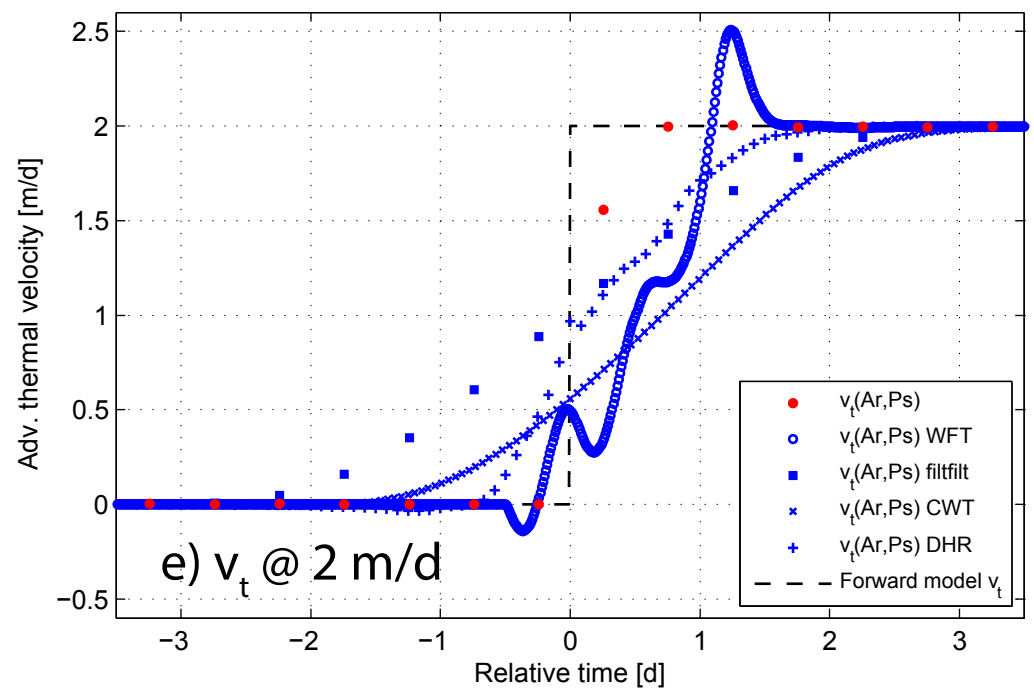
e) v_t @ 2 m/d
Adv. thermal velocity [m/d]
Relative time [d]
v_t(Ar,Ps)
v_t(Ar,Ps) WFT
v_t(Ar,Ps) filtfilt
v_t(Ar,Ps) CWT
v_t(Ar,Ps) DHR
Forward model v_t

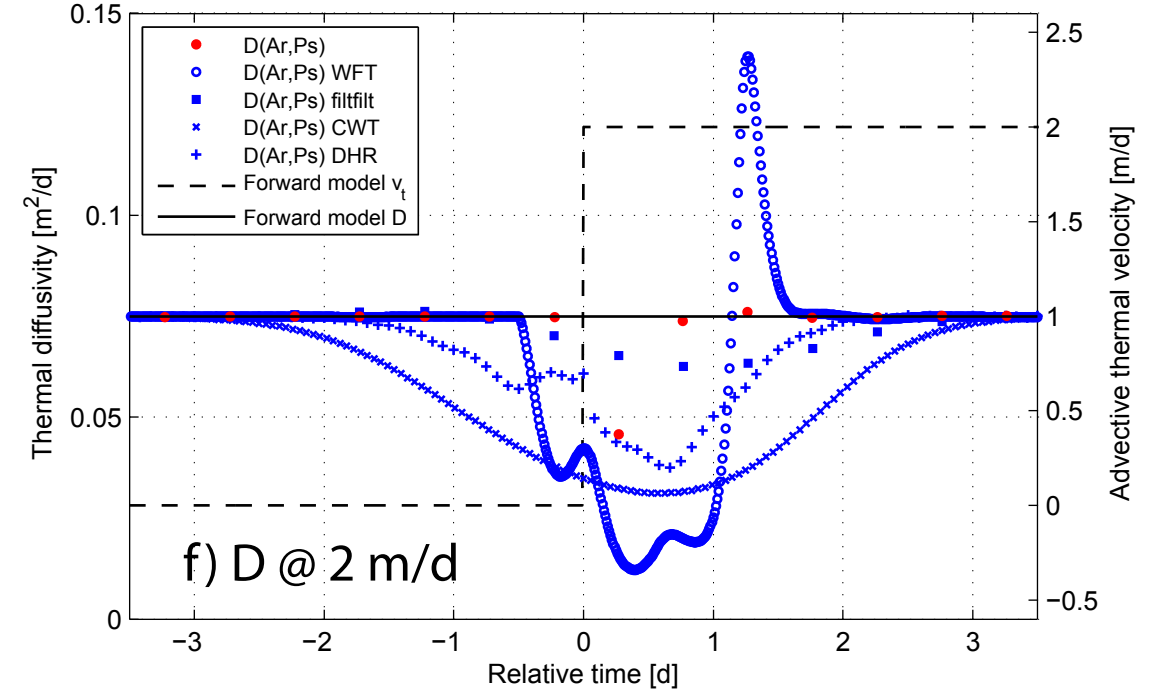
f) D @ 2 m/d
Thermal diffusivity [m²/d]
Advective thermal velocity [m/d]
Relative time [d]
D(Ar,Ps)
D(Ar,Ps) WFT
D(Ar,Ps) filtfilt
D(Ar,Ps) CWT
D(Ar,Ps) DHR
Forward model v_t
Forward model D

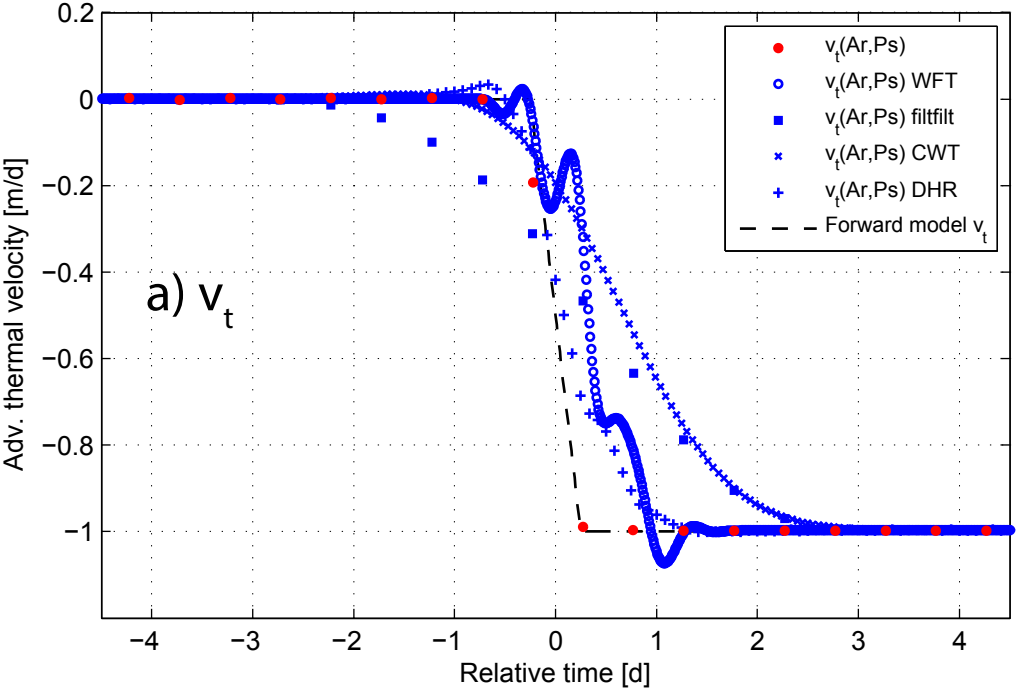
a) v_t
Adv. thermal velocity [m/d]
Relative time [d]
v_t(Ar,Ps)
v_t(Ar,Ps) WFT
v_t(Ar,Ps) filtfilt
v_t(Ar,Ps) CWT
v_t(Ar,Ps) DHR
Forward model v_t

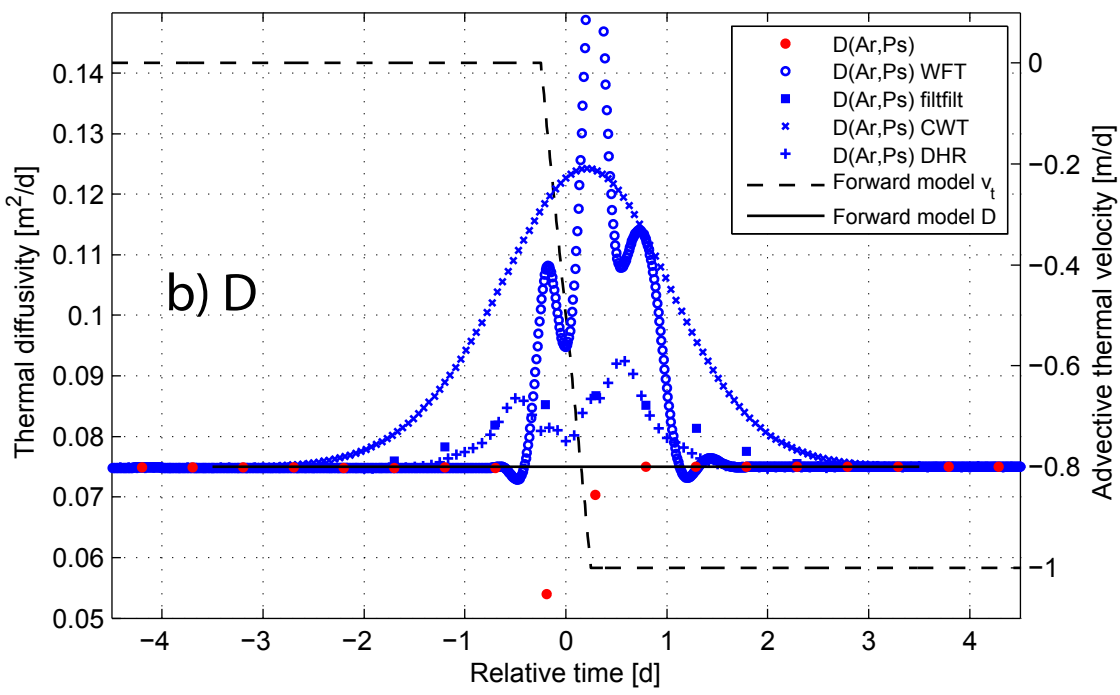
b) D
Thermal diffusivity [m²/d]
Advective thermal velocity [m/d]
Relative time [d]
D(Ar,Ps)
D(Ar,Ps) WFT
D(Ar,Ps) filtfilt
D(Ar,Ps) CWT
D(Ar,Ps) DHR
Forward model v_t
Forward model D

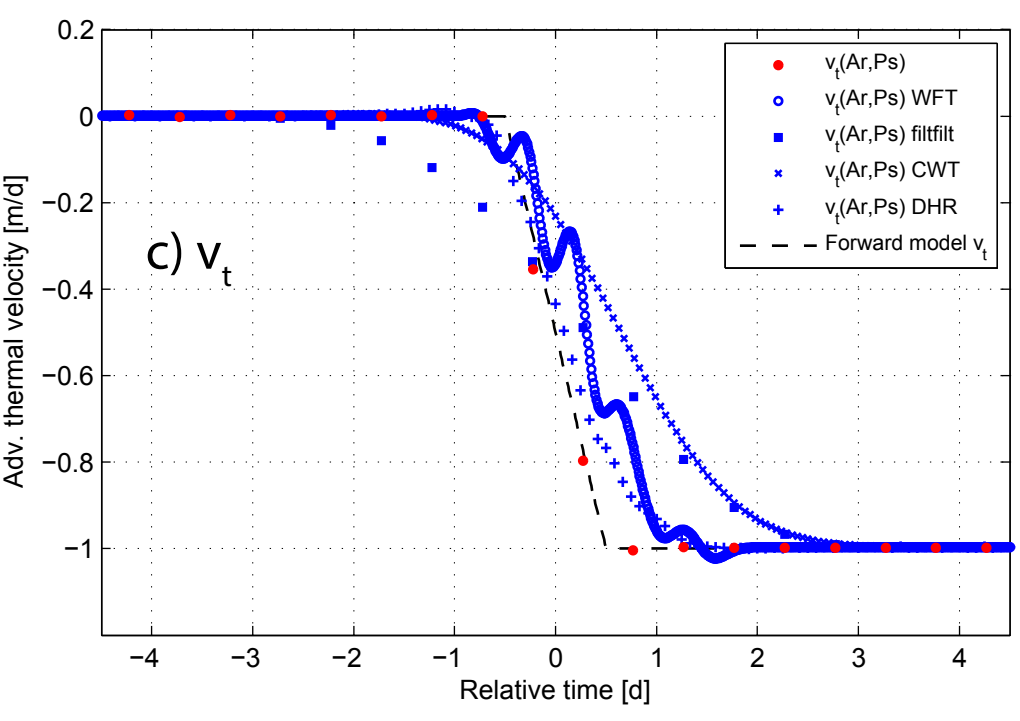
c) v_t
Adv. thermal velocity [m/d]
Relative time [d]
v_t(Ar,Ps)
v_t(Ar,Ps) WFT
v_t(Ar,Ps) filtfilt
v_t(Ar,Ps) CWT
v_t(Ar,Ps) DHR
Forward model v_t

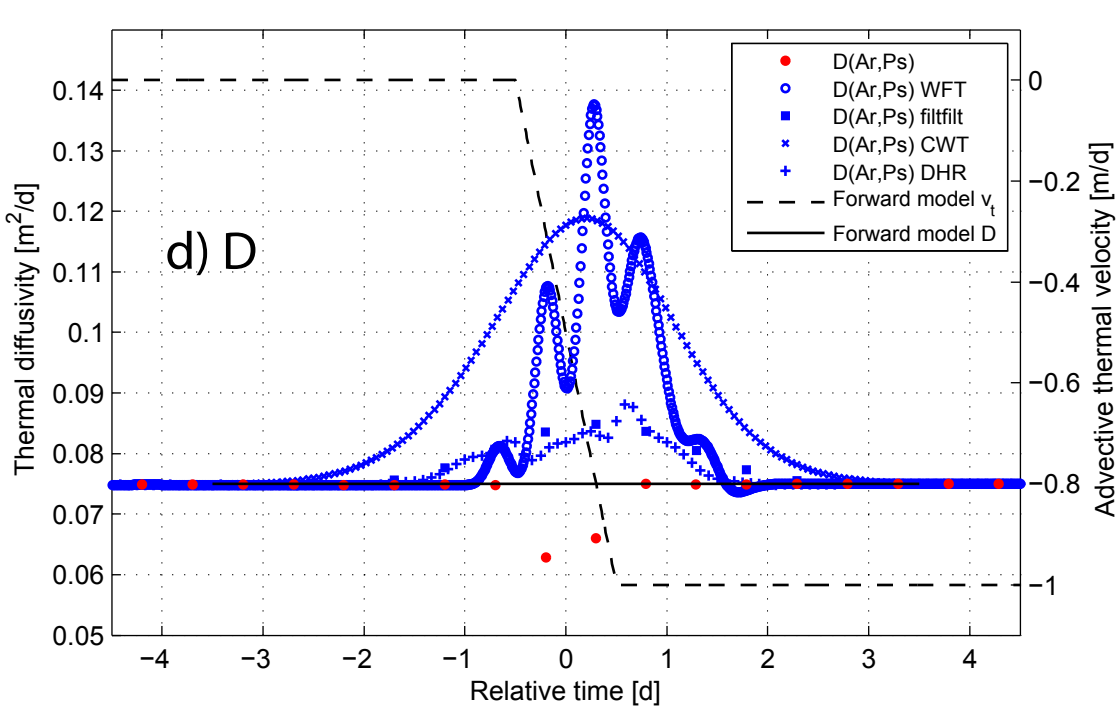
d) D
Thermal diffusivity [m²/d]
Advective thermal velocity [m/d]
Relative time [d]
D(Ar,Ps)
D(Ar,Ps) WFT
D(Ar,Ps) filtfilt
D(Ar,Ps) CWT
D(Ar,Ps) DHR
Forward model v_t
Forward model D

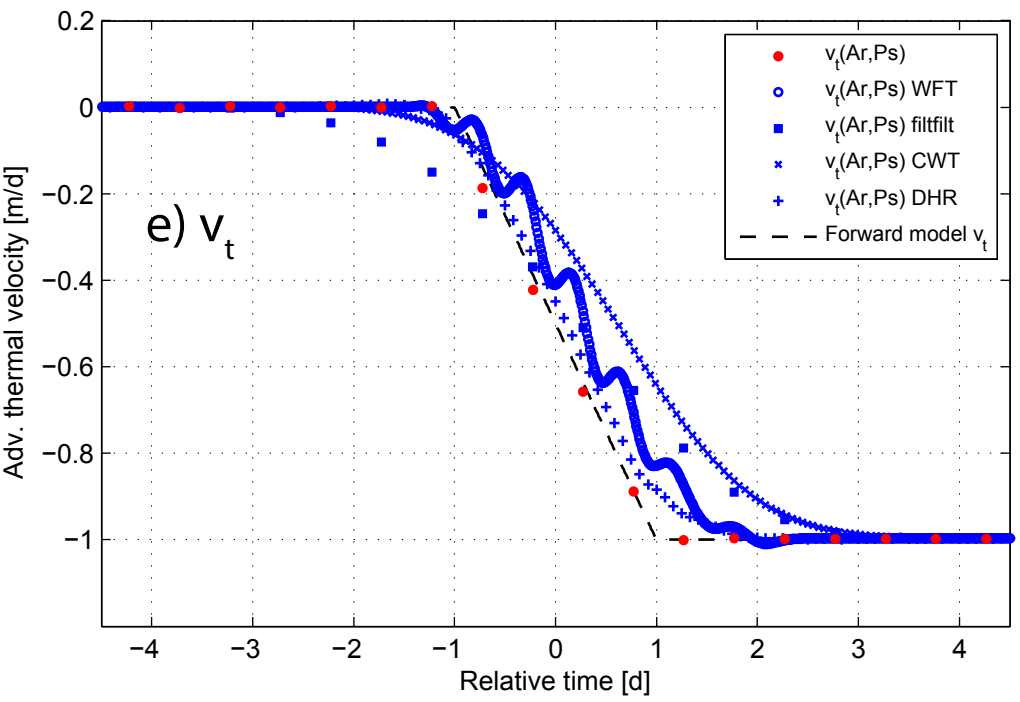
e) v_t
Adv. thermal velocity [m/d]
Relative time [d]
v_t(Ar,Ps)
v_t(Ar,Ps) WFT
v_t(Ar,Ps) filtfilt
v_t(Ar,Ps) CWT
v_t(Ar,Ps) DHR
Forward model v_t

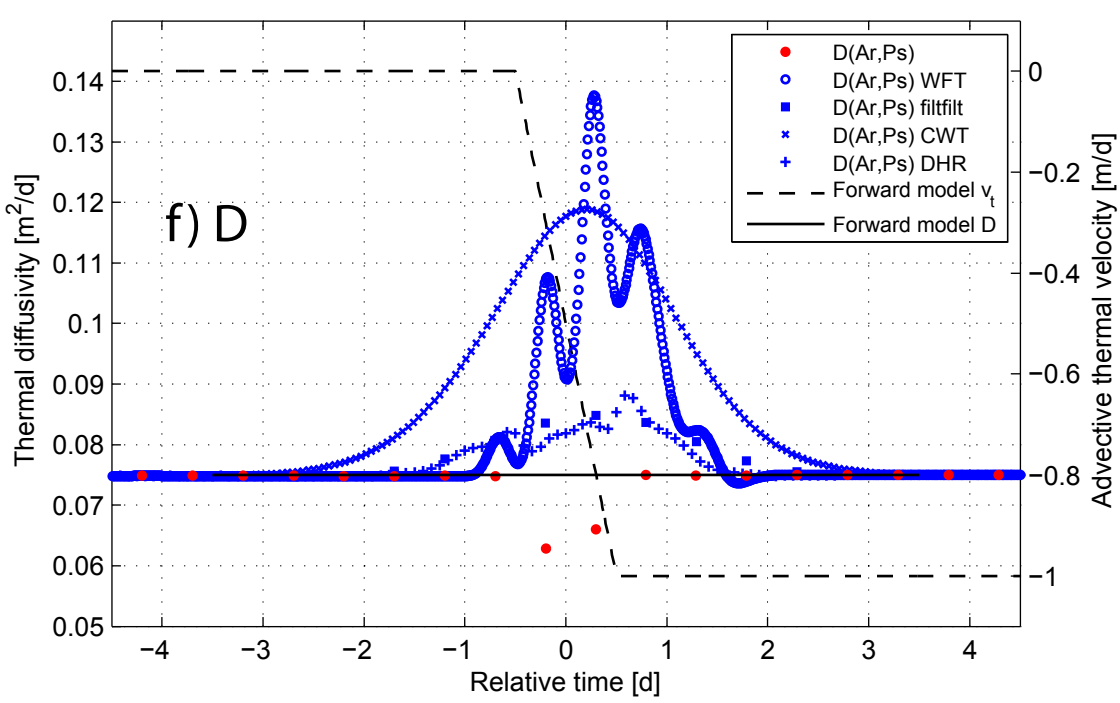
f) D
Thermal diffusivity [m²/d]
Advective thermal velocity [m/d]
Relative time [d]
D(Ar,Ps)
D(Ar,Ps) WFT
D(Ar,Ps) filtfilt
D(Ar,Ps) CWT
D(Ar,Ps) DHR
Forward model v_t
Forward model D

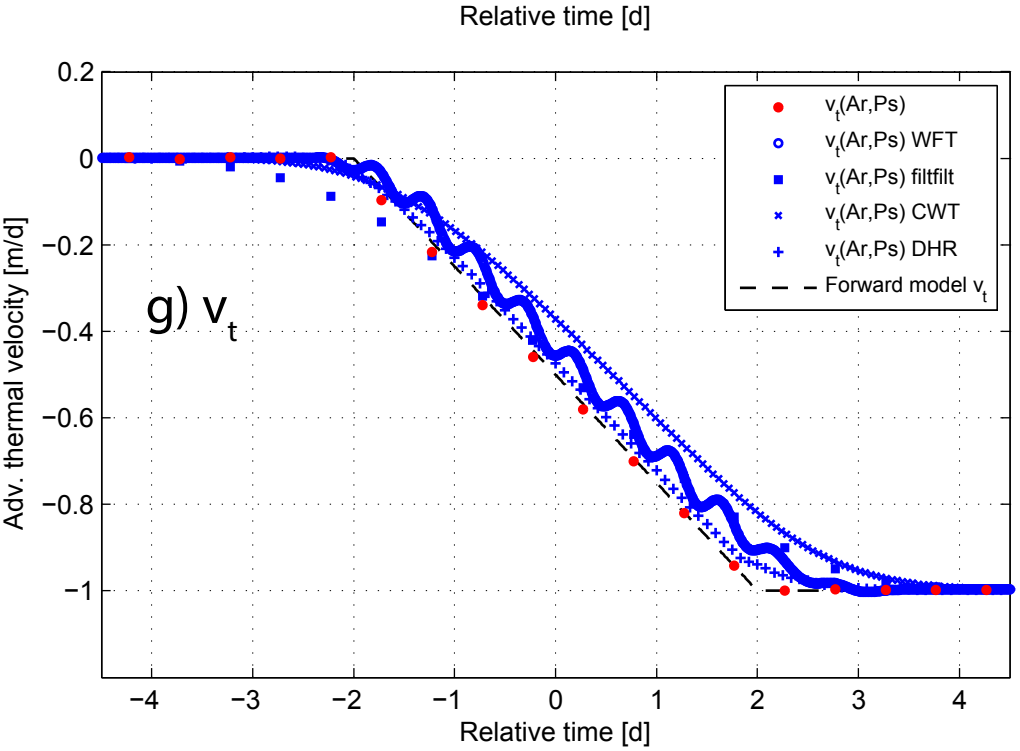
g) v_t
Adv. thermal velocity [m/d]
Relative time [d]
v_t(Ar,Ps)
v_t(Ar,Ps) WFT
v_t(Ar,Ps) filtfilt
v_t(Ar,Ps) CWT
v_t(Ar,Ps) DHR
Forward model v_t

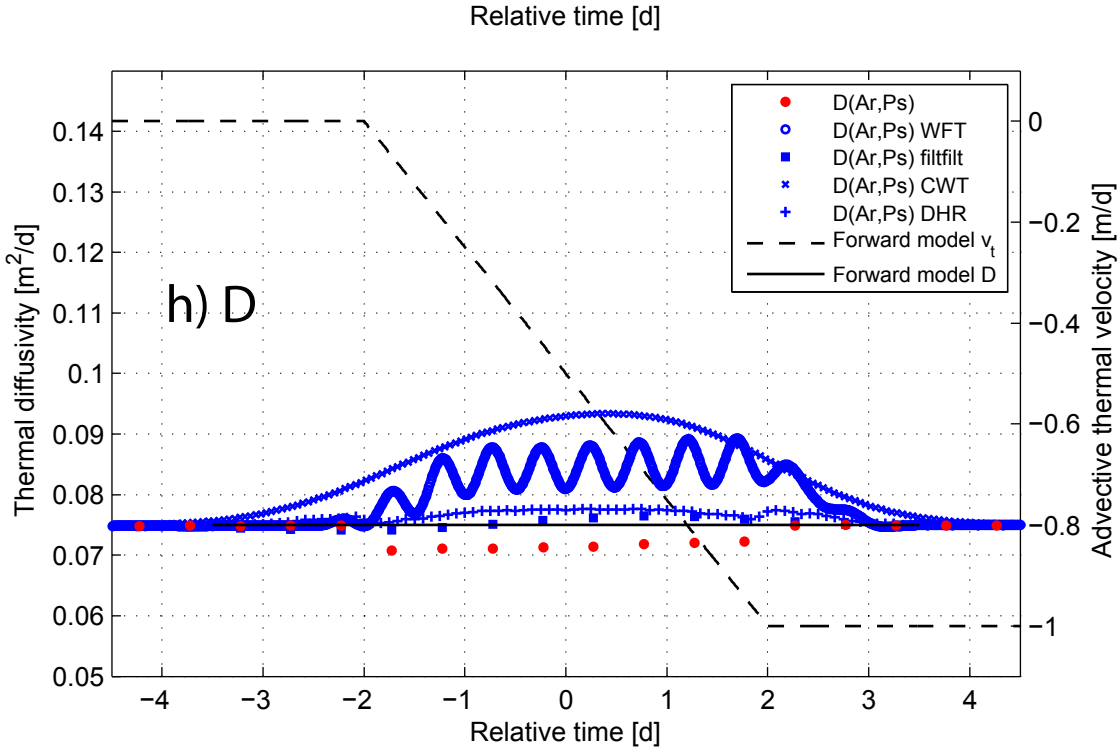
h) D
Thermal diffusivity [m²/d]
Advective thermal velocity [m/d]
Relative time [d]
D(Ar,Ps)
D(Ar,Ps) WFT
D(Ar,Ps) filtfilt
D(Ar,Ps) CWT
D(Ar,Ps) DHR
Forward model v_t
Forward model D

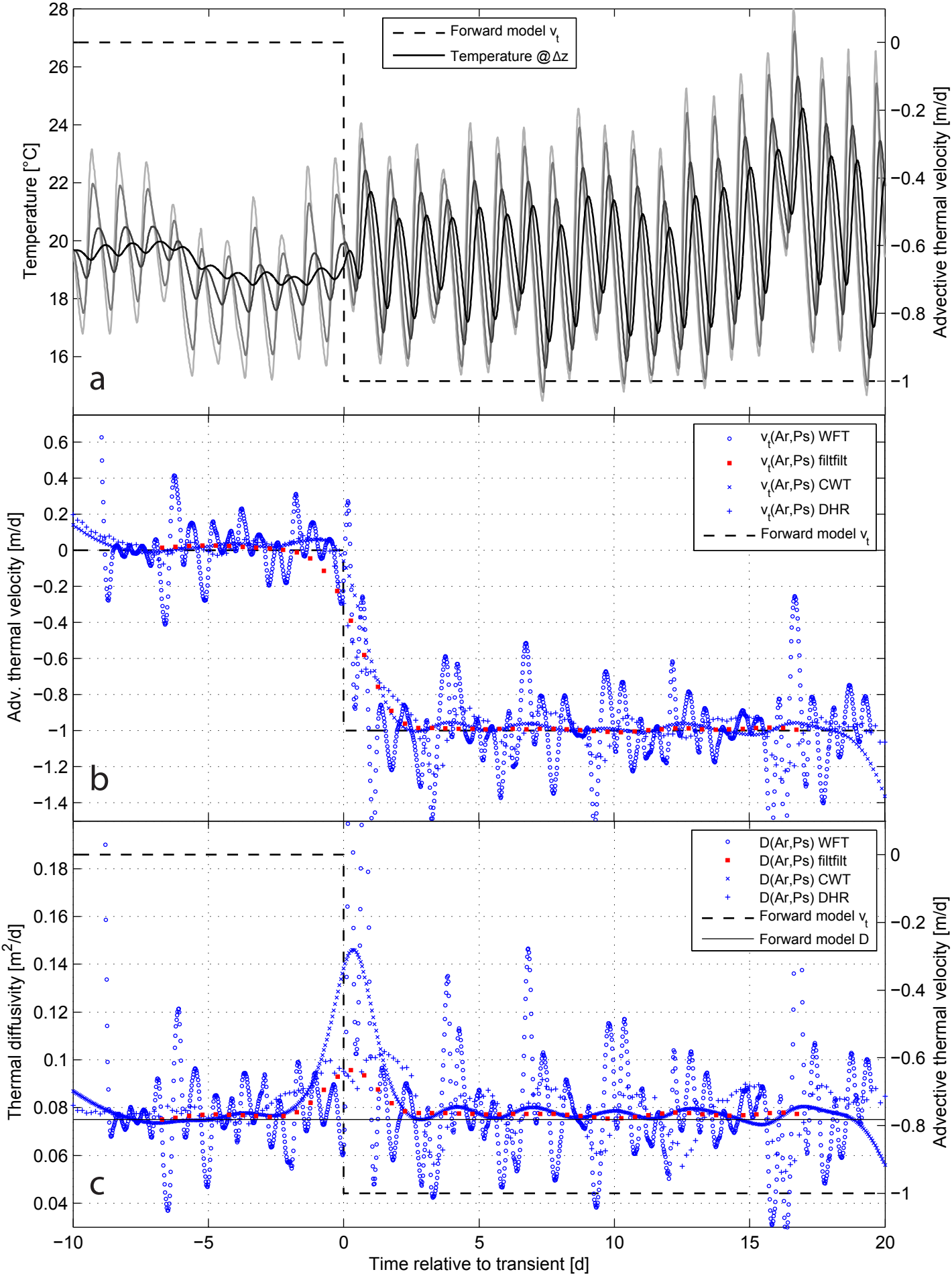
Forward model v_t
Temperature @Δz
Temperature [°C]
Advective thermal velocity [m/d]
a
v_t(Ar,Ps) WFT
v_t(Ar,Ps) filtfilt
v_t(Ar,Ps) CWT
v_t(Ar,Ps) DHR
Forward model v_t
Adv. thermal velocity [m/d]
b
D(Ar,Ps) WFT
D(Ar,Ps) filtfilt
D(Ar,Ps) CWT
D(Ar,Ps) DHR
Forward model v_t
Forward model D
Thermal diffusivity [m²/d]
Advective thermal velocity [m/d]
c
Time relative to transient [d]

Rate of velocity change dv/dt [L/T^2]	Max. thermal velocity error [m/d]					RMSE [ºC]				
	No filter	WFT	filtfilt	CWT	DHR	No filter	WFT	filtfilt	CWT	DHR
-0.25	-0.03	0.12	0.11	0.18	0.06	0.011	0.050	0.055	0.090	0.020
-0.5	-0.05	0.21	0.23	0.36	0.12	0.015	0.069	0.098	0.130	0.030
-1	-0.08	0.40	0.35	0.56	0.23	0.019	0.098	0.134	0.167	0.049
-2	-0.13	0.75	0.53	0.70	0.31	0.031	0.134	0.181	0.193	0.067
-∞	-0.04	0.99	0.50	0.83	0.57	0.011	0.208	0.177	0.247	0.134

Table 1: Summary of maximum error and root mean square error (RMSE) calculated from modeled and inverted advective thermal velocities using unfiltered and filtered temperature data for the same magnitude velocity transients (0 to -1 m/d) but for different rates of velocity change. The values in this table represent a quantification of the results in Figure 8a, 8c, 8e, 8g and Figure 5a.

Rate of velocity change dv/dt [L/T^2]	Max. thermal diffusivity error [m^2/d]					RMSE [ºC]				
	No filter	WFT	filtfilt	CWT	DHR	No filter	WFT	filtfilt	CWT	DHR
-0.25	-0.004	0.014	0.001	0.018	0.003	0.002	0.006	0.001	0.011	0.002
-0.5	-0.008	0.030	0.005	0.032	0.006	0.003	0.010	0.002	0.014	0.002
-1	-0.012	0.063	0.010	0.044	0.013	0.004	0.014	0.004	0.018	0.004
-2	-0.021	0.097	0.012	0.049	0.017	0.005	0.018	0.005	0.020	0.005
-∞	0.000	0.156	0.014	0.056	0.025	0.000	0.031	0.006	0.026	0.008

Table 2: Summary of maximum error and root mean square error (RMSE) calculated from modeled and inverted thermal diffusivities using unfiltered and filtered temperature data for the same magnitude velocity transients (0 to -1 m/d) but for different rates of velocity change. The values in this table represent a quantification of the results in Figure 8b, 8d, 8f, 8h and Figure 5b.